REFLECTOR ANTENNAS

Reflector antennas have been of importance for decades in several areas of electrical engineering, ranging from telecommunications and radars to deep-space exploration and radio astronomy. This is due to the high gain of reflector antennas, typically above 30 dBi. If we extend the concept of a reflector antenna to a reflecting mirror and view the human eye as the feed antenna operating in receiving mode, reflector antennas have been known for centuries. Optical astronomers have long been using reflecting mirrors in telescopes to enhance the visibility of stars, planets, and other celestial bodies.

The basic principle of operation of a parabolic reflector is that all rays emanating radially from a point source located at the focal point are reflected as a concentrated bundle of parallel rays, which can propagate for very long distances without loss due to speading. Inversely, incident rays parallel to the axis of symmetry of the paraboloid are all reflected toward its focal point, which concentrates the received signal at a single point. In that case, if the human eye or camera is placed a little bit behind the reflector focal point, an image with enhanced luminosity and definition is formed (Fig. 1).

However, reflector antennas can be designed to be wideband devices, not limited to operation at frequencies covered by the spectrum of visible light. Radio telescopes, for example, search for celestial radio sources over a wide range of frequencies (e.g., 300 MHz to 40 GHz). In this case, the radio sources and corresponding frequencies are marked on charts ac-

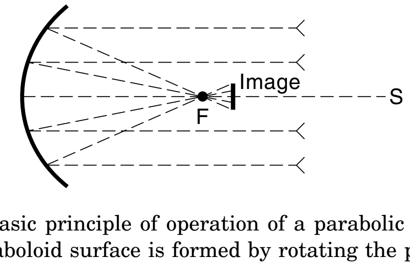

Figure 1. Basic principle of operation of a parabolic reflecting mirror. The paraboloid surface is formed by rotating the parabolic curve about its axis of symmetry (s axis).

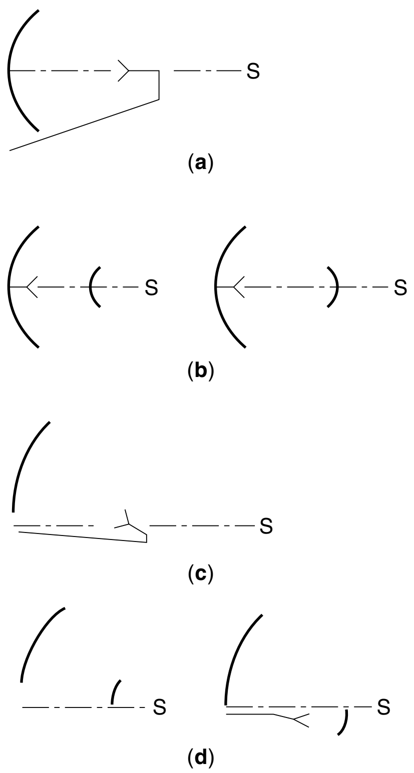

Figure 2. The evolution of reflector antenna systems: (a) single axisymmetric reflector, (b) dual axisymmetric reflector, (c) single offset reflector, and (d) dual offset reflector. The main reflectors are parabolic.

cording to their physical locations in the sky, forming maps similar to the ones elaborated by optical astronomers. Feed antennas are employed to receive the signals from the celestial radio sources at different bandwidths.

One of the first reflector antennas operating at radio frequencies was built by Hertz in 1888 and consisted of a sheet of zinc of about 2 m by 1.2 m, molded as a parabolic cylinder and illuminated by a dipole feed (1). Since then, reflector antenna technology has gradually evolved toward the state of the art known today for the purpose of improving electrical performance and/or simplifying mechanical structure (Fig. 2). The most basic form is the single axisymmetric parabolic reflector shown in Fig. 2(a), which is still in widespread use primarily at low frequencies and for low-cost applications. Large reflectors frequently use an axisymmetric dual reflector system with a parabolic main reflector, as shown in Fig. 2(b). The subreflectors are hyperbolic (Cassegrain system) or elliptical (Gregorian system). These systems offer a shorter transmission line (or waveguide) run to the feed antenna and are often used as earth terminal antennas in satellite communication networks.

Axisymmetric single and dual reflectors suffer from aperture blockage due to the presence of feed/subreflector and supporting mechanical structures in front of the main reflector aperture. This problem is solved by using an offset system with a main reflector that is a section of a parent reflector, normally a paraboloid of revolution, as shown in Fig. 2(c) and (d). Design and construction of offset reflectors are more elaborate than for their symmetrical counterparts.

Remarkable technological advancements were achieved during World War II, as reflectors were widely employed in radar and communication systems (2). However, it was only with the proliferation of digital computers in the late 1960s that the most accurate analysis and synthesis algorithms were developed, especially the ones related to the configurations of Fig. 2(c,d) and (3–7). Closed-form analysis algorithms are generally only applied to symmetrical reflectors (4,8).

In addition, substantial improvements on the electrical performance of both axisymmetric and offset dual reflector configurations were obtained with shaping algorithms, an effort only possible with efficient numerical processing combined with a solid knowledge of differential geometry and electromagnetics (5,9,10). The axisymmetric dual shaped reflector was introduced in the 1970s (9) and is popular for large earth station antennas. The offset dual shaped reflector has reportedly achieved aperture efficiencies of about 85% (11) and has been enjoying an increase in popularity. As a consequence, the analysis and design of reflector antennas is nowadays a specialized and unique area in applied electromagnetics, occupying many distinguished workers in industry and academia.

For the past two decades, reflector antennas have been applied primarily to satellite communications and networks, deep-space exploration, and electronics defense. The reflector antenna carried by the Voyager spacecraft, for example, is a dual-reflector antenna shaped for high gain (Fig. 3). Besides specific designs applied to unique purposes, such as spacecrafts and radiotelescopes, reflector antennas are also being produced on a very large scale for commercial applications, a multimillion-dollar market directly related to the globalization of communication currently underway. In particular, VSAT systems (very small-aperture terminals) are proliferating and connecting together branches of large corporations, such as chains of stores, banks, and car manufacturers. The VSAT market is expected to grow at a rate of 20% per year (12).

Other examples of substantial economic importance are the satellite-based cellular communication systems, such as the Motorola IRIDIUM, in which well-defined multibeam coverage is required, and direct-to-home (DTH) satellite TV systems, such as Hughes DirecTV and others, which employ small offset parabolic antennas to receive satellite signals. Thus, reflector antennas are present in our lives as major gateways for the exchange of information at home and, less conspicuously, in defense systems. Reflector antennas can therefore be considered one of the most successful electrical devices of all time, in view of their importance in many modern engineering systems and applications, such as cellular communications, satellite TV, and electronic defense, as well as in the exploration of our galaxy and beyond.

THE PARABOLIC REFLECTOR ANTENNA AND OTHER SINGLE-REFLECTOR SYSTEMS

Preliminary Considerations and Geometry

Single-reflector systems, such as the parabolic reflector antenna, consist of a reflecting surface illuminated by a feed antenna, usually a horn. It is necessary to know the radiation characteristics of the feed antenna in order to evaluate correctly the electrical performance of the reflector system. A

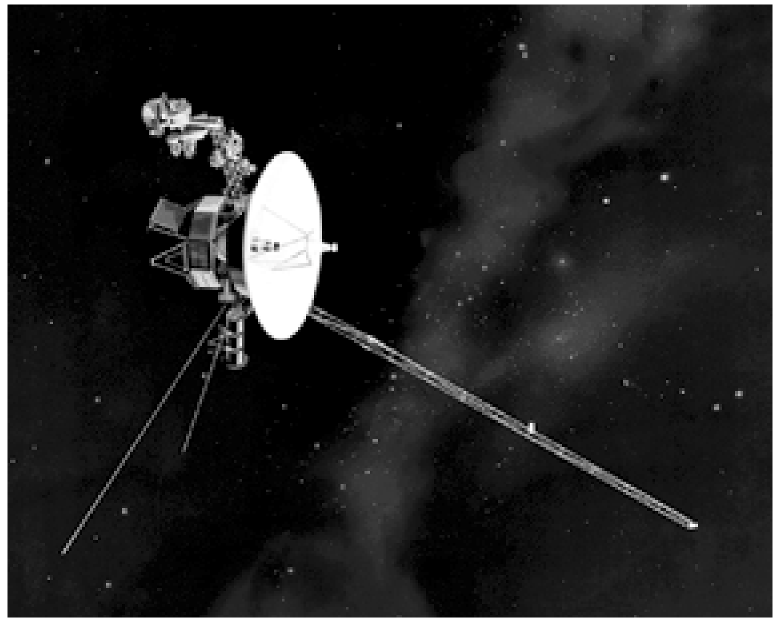

Figure 3. Full-scale model of one of the twin Voyager spacecraft. Note at the center the dual-shaped, high-gain reflector antenna employing a main reflector with a diameter of 3.66 m (12 ft). (Courtesy Jet Propulsion Laboratory. Copyright © California Institute of Technology, Pasadena, CA. All rights reserved. Based on government-sponsored research under contract NAS7-1260.)

more detailed discussion is presented in the section entitled "Feed Antennas." In the next few subsections we employ simple analytical models to describe the radiation properties of feed antennas. Once the feed pattern is known, the total radiation pattern of the reflector system can be obtained using the techniques described in the section entitled "Analysis Methods and Evaluation," in combination with the geometrical properties of the reflector itself, which is the main subject of this and following subsections.

The general geometry of a parabolic reflector is shown in Fig. 4, and all associate symbols are listed in Table 1. Figure 4 is a cross-section view of the three dimensional paraboloid, which is formed by rotating the parabolic curve shown in Fig. 4 about its axis of symmetry (s axis). If the rotation is performed with $H = 0$, an axisymmetric paraboloid of diameter D_p is formed. Otherwise, an offset reflector is generated. We limit our analytical analysis to parabolic reflectors with circular projected diameters. However, other shapes, such as elliptical, are also used in practice to some extent, especially as earth-station antennas in communication links with synchronous satellites. An effort is made to discuss this and other types of reflector antennas.

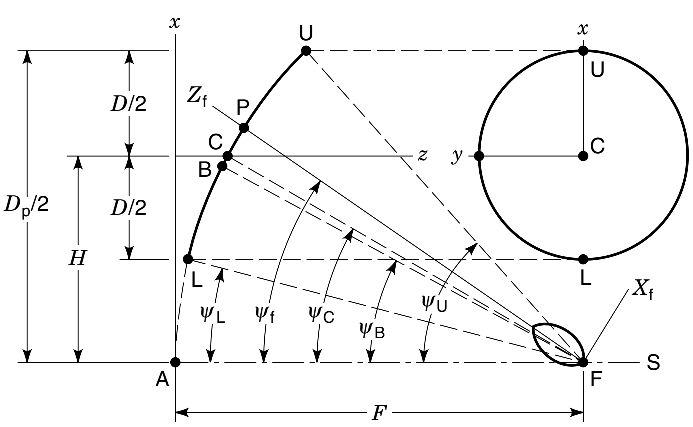

Figure 4. Geometry for the axisymmetric ($H = 0$) and offset parabolic reflector. See Table 1 for definitions of parameters.

Basic Equations

First we consider the axisymmetric parabolic reflector, which is obtained from Fig. 4 for $H = 0$ and $\psi_f = 0°$ (i.e., the feed

Table 1. Definitions of Symbols for Single Configuration

Symbol	Definition
D	Diameter of the projected aperture of the parabolic main reflector ($D = D_p$ for an axisymmetric paraboloid)
D_p	Diameter of the projected aperture of the parent paraboloid
H	Offset of reflector center ($H = 0$ for an axisymmetric paraboloid)
F	Paraboloid focal length
Point F	Focal point
Point A	Apex of the parent paraboloid
Point B	Point on main reflector that bisects subtended angle viewed from focal point
Point C	Point on main reflector that projects to the center of the projected aperture
Point P	Point on main reflector corresponding to the ray arising from the peak of the feed pattern
ψ_f	Angle of feed antenna pattern peak relative to reflector axis of symmetry s (feed is aimed at point P)
ψ_B	Value of ψ_f that bisects the reflector subtended angle (i.e., feed is aimed at point B)
ψ_F	Value of ψ_f when the feed is aimed at the reflector point C corresponding to the aperture center
$\psi_U - \psi_L$	Angle subtended by the parabolic main reflector as viewed from the focal point

antenna main beam peak is aimed at the reflector apex, point A). For this particular case, D_p is the diameter of the projected aperture and the aperture plane is the $x_f y_f$ plane, in which we define polar coordinates (ρ_f, ϕ_f). Furthermore, we associate the spherical coordinates (r_f, θ_f, ϕ_f) with the rectangular system $x_f y_f z_f$ shown in Fig. 4. The parabolic curve can then be expressed at any ϕ_f as

$$r_f = \frac{2F}{1+\cos\theta_f} = F\sec^2\frac{\theta_f}{2} \tag{1}$$

or

$$F - r_f\cos^2\frac{\theta_f}{2} = 0 \tag{2}$$

and the projection of r_f onto the aperture plane is

$$\rho_f = r_f\sin\theta_f = 2F\tan\theta_f \tag{3}$$

which yields $\rho_f = 0$ at the reflector apex ($\theta_f = 0°$) and $\rho_f = D_p/2$ at the reflector edge ($\theta_f = \psi_0 = \psi_L = \psi_U$).

The axisymmetric paraboloid is completely specified in terms of its diameter D_p and curvature rate F/D_p. The greater is F/D_p, the flatter is the reflector. Common values are usually between 0.25 and 1.0. At the reflector edge, Eq. (3) becomes $D_p/2 = 2F\tan\psi_0$, which yields

$$\psi_0 = 2\tan^{-1}\frac{1}{4F/D_p} \tag{4}$$

The unit vector $\hat{\boldsymbol{n}}$ normal to the parabolic surface, can be found by normalizing the gradient of Eq. (2) and is given by

$$\hat{\boldsymbol{n}} = -\hat{\boldsymbol{r}}_f\cos\frac{\theta_f}{2} + \hat{\boldsymbol{\theta}}_f\sin\frac{\theta_f}{2} \tag{5}$$

The angle α_i between the surface normal, given by Eq. (5), and an incident ray coming from the focal point can then be calculated from

$$\cos\alpha_i = -\hat{\boldsymbol{r}}_f\cdot\hat{\boldsymbol{n}} = \cos\frac{\theta_f}{2} \tag{6}$$

Finally, the angle α_r between the correspondent reflected ray and surface normal can be determined by enforcing the law of reflection on the reflector surface; that is, $\alpha_r = \alpha_i$. Thus

$$\cos\alpha_r = \cos\frac{\theta_f}{2} = \hat{\boldsymbol{z}}\cdot\hat{\boldsymbol{n}} \tag{7}$$

where $\hat{\boldsymbol{z}} = -\hat{\boldsymbol{r}}_f\cos\theta_f + \hat{\boldsymbol{\theta}}_f\sin\theta_f$. Equation (7) shows that all rays coming from the focal point F are reflected by the parabolic surface as a collimated beam parallel to the z axis, which is coincident with the s axis for the axisymmetric reflector. Thus the total path length from all rays coming from the focal point F to the aperture plane is given by

$$r_f + r_f\cos\theta_f = r_f(1+\cos\theta_f) = 2F \tag{8}$$

where Eq. (1) was employed in the derivation. Equation (8) shows that the total path length is constant, and we conclude that the phase distribution of a wave coming from a point source located at the focal point of a parabolic reflector will be constant across the aperture plane after reflection. This result yields another very important property of parabolic reflectors—that is, a parabolic reflector illuminated by a feed antenna with a unique phase center located at the focal point produces a uniform phase distribution across the aperture plane. As already seen, the beam is also collimated, forming a section of a plane wave. Nevertheless, the amplitude distribution is not uniform. In general, reaching a maximum at the center of the projected aperture and decreasing toward the edges of the axisymmetric paraboloid.

These basic properties make parabolic reflectors so widely used as reflector antennas. Although herein derived for the axisymmetric paraboloid, they are also valid for the offset case (i.e., $H \neq 0$ in Fig. 4). Offset reflectors offer significantly reduced aperture blockage, as the feed is not directly in front of the reflector, although it is still located at the focal point F, yielding higher gains than do axisymmetric reflectors of similar aperture sizes. From Fig. 4 we see that the feed needs to be tilted by an angle ψ_f in order to direct its pattern toward the offset reflector; otherwise large spillover (i.e., feed radiation missing the reflector) and associated gain loss are introduced. In many systems, the feed pointing angle ψ_f is set equal to the angle that bisects the reflector, ψ_B, or to the angle pointed toward the center of the projected aperture, ψ_C. The influence of the feed pointing angle ψ_f on the electrical characteristics of offset parabolic reflector antennas is discussed in the section entitled "Design of Axisymmetric and Offset Parabolic Reflector Antennas." The angles shown in Fig. 4 are obtained from the following relations:

$$\psi_L = 2\tan^{-1}\frac{4H - D_p}{4F} \tag{9}$$

$$\psi_U = 2\tan^{-1}\frac{1}{4F/D_p} \tag{10}$$

$$\psi_B = \frac{\psi_L + \psi_U}{2} \tag{11}$$

$$\psi_C = 2\tan^{-1}\frac{H}{2F} \tag{12}$$

with

$$D_p = D + 2H \tag{13}$$

As we see, there are many parameters necessary to specify completely a parabolic reflector antenna. However, before we design reflector systems, it is necessary to study a few of their characteristics and properties. This knowledge is essential for selecting appropriate configurations for specific applications. Long-distance and frequency-reuse communication systems, for example, require antennas with high gain and low cross polarization. Reflector antennas are particularly suitable for such applications due to their high gain. However, an in-depth understanding of their depolarization characteristics is necessary in order to achieve designs that guarantee a suitable isolation between orthogonally polarized channels in frequency-reuse systems. This and other properties that are almost exclusive to reflector antennas are discussed next.

Cross Polarization, Beam Squint, and Beam Deviation

Cross Polarization. Polarization is a basic characteristic of an electromagnetic wave and describes the motion of the electric field vector at a fixed point in space as a function of time. The polarization of an antenna is the polarization of its radiated wave when operating in the transmitting mode. Generally, the polarization of any antenna system can be decomposed into two orthogonal components in the far field, referred to as copolarization and cross polarization. In the particular case of reflector antenna systems, the copolarization is usually taken to be the polarization presented by the feed antenna illuminating the reflector. As a consequence, the cross polarization is orthogonal to the feed-antenna main polarization. This agrees with Ludwig's third definition of cross polarization (13) and is the one herein employed. The cross-polarization (XPOL) level is defined quantitatively as the ratio of the peak in the cross-polarized radiation pattern to the peak value of the copolarized pattern (i.e., the main beam peak), usually expressed in decibels.

As previously mentioned, reflector antennas cannot be properly evaluated without first describing the feed antenna. A detailed discussion about modeling feeds is presented in the section titled "Feed Antennas." Here we employ an analytical model that, despite its simplicity, approximates reasonably well the copolarized radiation properties of feeds usually encountered in practice, such as conical corrugated horns. The radiation pattern $\boldsymbol{E}_f$ of an idealized balanced feed (i.e., the primary radiation is symmetric in ϕ_f) with a fixed phase center can be described by (3)

$$\boldsymbol{E}_{\mathrm{f}} = \frac{e^{-jkr_{\mathrm{f}}}}{r_{\mathrm{f}}} C(\theta_{\mathrm{f}})[\hat{\theta}_{\mathrm{f}} \cos\phi_{\mathrm{f}} - \hat{\boldsymbol{\phi}}_{\mathrm{f}} \sin\phi_{\mathrm{f}}] \tag{14}$$

where k is the free-space wave number $2\pi/\lambda$ and

$$C(\theta_{\mathrm{f}}) = G_0\, 10^{(\mathrm{FT}/20)(\theta_{\mathrm{f}}/\theta_{\mathrm{f0}})^2} \tag{15}$$

where FT is the feed taper in decibels at $\theta_f = \theta_{f0}$ and the gain normalization constant G_0 is found by numerical integration of Eq. (15); see Ref. 14 for further details. We first examine the axisymmetric reflector of Table 2 using a balanced feed as described by Eq. (14), which is purely linearly polarized (LP) along the x axis, with the Gaussian pattern of Eq. (15) yielding a 10 dB beamwidth of 70° (i.e., FT = 10 and θ_{f0} = 35°). A y_f-polarized feed pattern can be obtained from Eq. (14) by replacing the argument ϕ_f with $\phi_f - \pi/2$. In addition, a circularly polarized feed is obtained by combining the x_f-polarized pattern in Eq. (14) with a y_f-polarized pattern that is in phase quadrature (i.e., multiplied by a factor of j). The physical optics portion of the commercial code GRASP (general reflector antenna synthesis package, TICRA Engineering) is used to compute the radiation patterns (14). The physical optics formulation applied to the analysis of reflector antennas is discussed in the section entitled "Analysis Methods and Evaluation."

Table 2. Axisymmetric and Offset Parabolic Reflector Configurations

Reflector Configuration	*Axisymmetric*	*Offset*
Shape:	Parabolic	Parabolic
Projected diameter D:	171λ	85.5λ
Parent reflector diameter D_p:	171λ	171λ
F/D_p:	0.3	0.3
Offset of reflector center, H:	0	42.75λ
	Feed Configuration (On Focus)	
Polarization:	Linear (x_f)	Linear (x_f)
Pattern shape:	Gaussian; Eqs. (14) and (15)	Gaussian; Eqs. (14) and (15)
Gain G_f (dBi):	14.04	14.04
10 dB beamwidth (deg):	70	70
Feed angle ψ_f(deg):	0	39.81

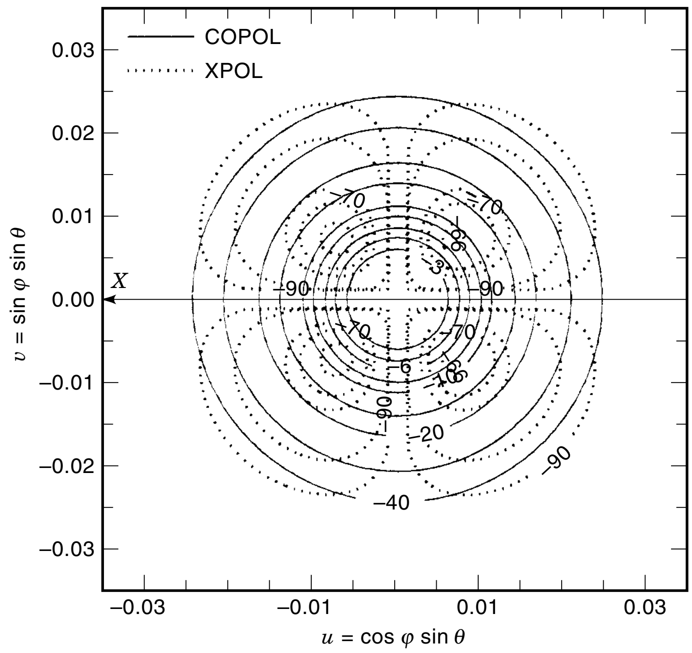

Figure 5. Contour plots in decibels of the computed co- and cross-polarized patterns of the 171λ diameter axisymmetric parabolic reflector specified in Table 2.

For the axisymmetric configuration of Table 2, the computed level of XPOL displayed in Fig. 5 is very low (a maximum of −65.35 dB below the main beam peak of 48.62 dBi). Typically, the feed assembly and supports, although not taken into account by the computer simulations, will create more XPOL than this. Although illustrated for a particular case, this is a general result (9), and we conclude that reflector-induced XPOL in axisymmetric reflectors illuminated by balanced feeds is often negligible. In addition, according to Fig. 5, the XPOL peaks are all located in the 45° planes.

The cross-polarization behavior of offset reflectors is illustrated with a derivative of the 171λ axisymmetric parent reflector of Table 2. A portion of the upper half of the axisymmetric reflector is retained, so that the offset reflector with a 85.5λ projected aperture diameter is just fully offset (i.e., the bottom of the reflector just touches its axis of symmetry). If the feed remains pointed at the apex of the parent paraboloid (i.e., ψ_f = 0°), negligible XPOL is generated (15). However, this leads to large spillover and associated gain loss. Therefore, in practice the feed is tilted to direct its pattern toward the reflector, resulting in the introduction of high XPOL.

The offset configuration of Table 2 is not symmetric about the yz plane, and therefore XPOL is not canceled in this plane as in the axisymmetric case. In fact, it is exactly in the yz plane that the peak XPOL levels occur. However, reflector

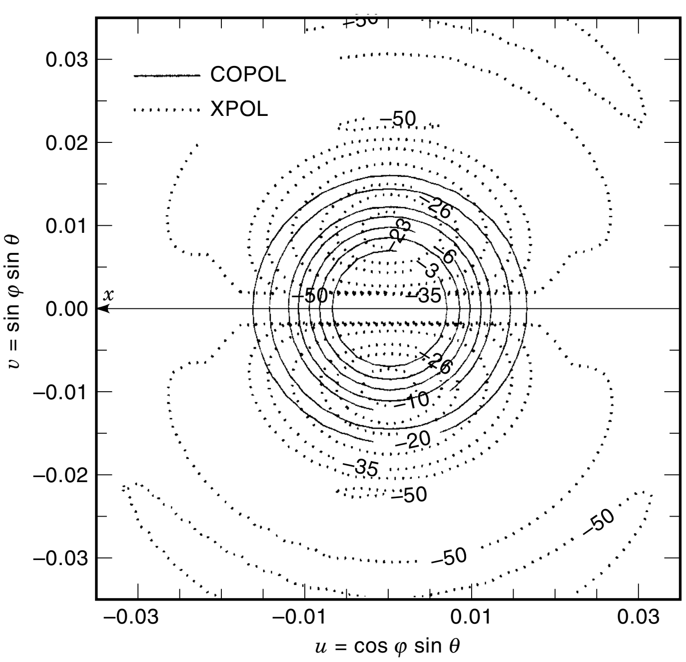

Figure 6. Contour plots in decibels of the computed co- and cross-polarized patterns of the 85.5λ diameter just fully offset parabolic reflector specified in Table 2.

symmetry is still present about the *xz* plane, and no substantial XPOL occurs in that plane. These results are demonstrated using the GRASP code for the offset reflector example with the XPOL contour plot shown in Fig. 6, for which the feed has a pointing angle of $\psi_f = \psi_B = 39.81°$, computed according to Eq. (11). The feed again has the pattern given by Eqs. (14) and (15), with a 10 dB beamwidth of 70°. The computed peak XPOL is −22.4 dB relative to the copolarized beam maximum of 47.39 dBi. Figure 6 indicates that the copolarized pattern is still symmetric, and the XPOL peaks are located at the copolar −6 dB contour line.

This example is typical of single offset reflectors and shows that single offset paraboloids illuminated by conventional feeds are limited by XPOL performance (9). It is worth noting that cross polarization arises from the reflector curvature and from the tilting of the feed. A planar reflector, for instance, does not depolarize an incident field coming in a direction perpendicular to the reflector. Thus we see that the XPOL decreases as the reflector curvature rate, F/D_p, increases. However, this reduction is not significant in offset reflectors, on account of the substantial feed tilting normally encountered in practice (15).

A XPOL level above −22 dB is often unacceptably high (3,7). In the section titled “Conditions for Minimizing Cross Polarization in Offset Cassegrain and Gregorian Systems” we discuss procedures to reduce XPOL in offset parabolic reflectors. Next we discuss an important property of parabolic reflector antennas that is inherently related to XPOL.

Beam Squint. As we have seen, offset reflectors offer significantly reduced aperture blockage but introduce high XPOL when illuminated by a LP feed. On the other hand, offset parabolic reflectors fed by a circularly polarized (CP) feed presenting a balanced radiation pattern do not have substantial XPOL. However, beam squint does occur (9,16); that is, the main beam peak squints off of the reflector axis in the plane perpendicular to the plane of symmetry (i.e., beam squint occurs in the *yz* plane of Fig. 4). The beam squints to opposite sides depending on the sense of the CP. Beam squint can be a major problem in satellite and deep-space communications if not carefully taken into account. A practical formula for the prediction of the beam squint angle θ_S in offset parabolic reflectors with on-focus CP feeds is (16)

$$\theta_S = \mp \sin^{-1}\left(\frac{\sin\psi_f}{2Fk}\right) \tag{16}$$

where F is the focal distance and k is the free-space wave number $2\pi/\lambda$. A negative θ_S means that the beam is squinted toward the left (left-hand CP feed), and a positive θ_S means a squint to the right (right-hand CP feed). Equation (16) shows that the amount of squinting is inversely proportional to the focal distance F. That is, longer-focal-length reflectors experience less beam squint. If the feed is displaced from the focal point, an equation similar to Eq. (16) is derived, as in Ref. 17. In offset parabolic configurations illuminated by off-focus CP feeds, beam squint occurs simultaneously with an effect called beam deviation, treated in the next subsection. Due to sense reversal encountered upon reflection from the main reflector, the sense of the far-field radiation is opposite to that of the feed (18). For example, a right-hand circularly polarized (RHCP) feed produces a left-hand circularly polarized (LHCP) radiation in the reflector far field, as illustrated next.

We consider as an example a just fully offset configuration with a diameter $D = 18.8\ \lambda$, $F/D_p = 0.25$, and $H = 9.4\ \lambda$, illuminated by a CP feed with a pattern of 10 dB beamwidth 70°. This geometry was selected because it is used in VSAT applications at 18.5 GHz and measured data are available (3,9). Figure 7 shows copolarized pattern cuts computed by GRASP (14) in the y–z plane with opposite-sense CP feeds. For a RHCP main beam (the feed is LHCP) the squint is to the left, as observed in Fig. 7. Likewise, the LHCP main beam squints to the right. From Fig. 7 we note that the angle be-

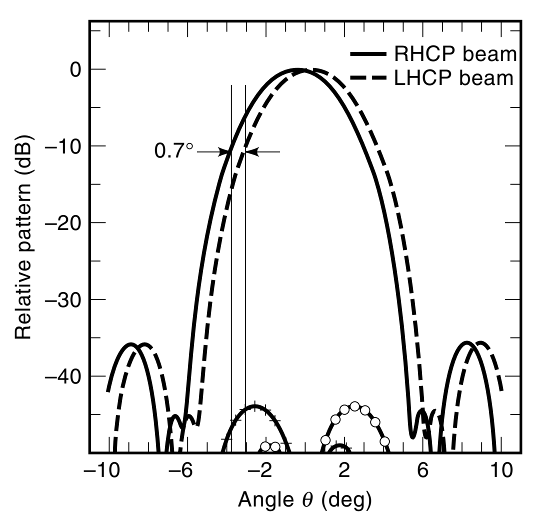

Figure 7. Computed RHCP and LHCP far-field patterns of an 18.8λ just fully offset parabolic reflector. Note the beam squint effect. The LHCP (circles) and RHCP (crosses) cross-polarized patterns are associated with the RHCP and LHCP beams, respectively.

tween the two beams (total beam separation) is 0.700°, which is in agreement with the value of 0.686° (2 θ_s) from Eq. (16). The reported measured value (3,9) is 0.750°. Finally, Fig. 7 also shows that circular XPOL is low (maximum of 42.71 dB below the gain of 33.88 dBi for any of the feed polarizations). The absence of circular XPOL in offset paraboloids with on-focus feeds is a general result, not limited to just fully offset paraboloids (17).

Although circular XPOL is low, there are substantial LP cross-polarized fields present at any given instant of time, in both the aperture distribution and the far-field pattern of the offset reflector (19). This and the fact that the orthogonal components of the incident field are not in phase (which is the case for a circularly polarized feed antenna) are the two necessary and sufficient conditions to generate beam squint (17). We now present a brief explanation of the beam squint generation mechanism.

The electric field components on the left side of the reflector ($y > 0$ in Fig. 4) always lead or lag in phase relative to the ones on the right side, depending on whether the primary field is LHCP or RHCP (19). This leads to a phase slope condition across the aperture, which squints the main beam to the left (negative angles in Fig. 7) or to the right (positive angles in Fig. 7). To illustrate the process, consider any two points in the projected aperture of the offset paraboloid that are equidistant from the reflector plane of symmetry. If the feed is LHCP, the electric field at those points rotates counterclockwise (RHCP main beam), as shown by Fig. 8. Thus, the electric field vector to the left is leading the one to the right, and as a final result (considering the influence of all points) the beam squints to the right (the view in Fig. 8). This is equivalent to a negative θ_S in Eq. (16), or to a squint to the left in the yz plane of the reflector coordinate system (negative angles in Fig. 7).

Beam Deviation. When a feed is laterally displaced from the focal point of a reflector, either axisymmetric or offset, the pattern main beam is scanned to the opposite side of the reflector axis. This is referred to as beam deviation, and it arises from a tipping of the aperture field phase plane relative to the reflector aperture plane. The main beam direction determined from these considerations is herein referred to as the reference axis; it is tilted from the reflector axis (i.e., the z axis in Fig. 4) according to the amount of feed displacement.

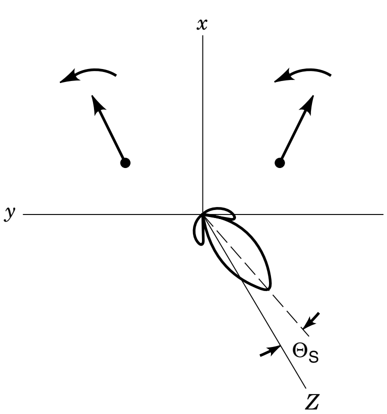

Figure 8. Beam squint generation mechanism.

Note that for an axisymmetric configuration the reflector and reference axes intersect at the apex of the parent paraboloid (point A in Fig. 4). If a CP feed is displaced from the focal point of an axisymmetric or offset paraboloid, both beam squint and deviation are present at the same time. Thus the amount of beam squint should be added to the reference axis in order to determine accurately the final position of the main beam.

For a feed displacement δ_f along the positive y_f direction in Fig. 4, the reference axis is tilted in the opposite direction from the reflector axis by an angle θ_D, computed according to

$$\theta_D = \mathrm{BDF}\tan^{-1}\frac{\delta_f}{F} \tag{17}$$

where BDF is the beam deviation factor, which can be approximately determined for small feed displacements δ_f, in axisymmetric and offset paraboloids, by (3,20)

$$\mathrm{BDF} = \frac{1 + 0.36\left(4\dfrac{F}{D_p - 2H}\right)^{-2}}{1 + \left(4\dfrac{F}{D_p - 2H}\right)^{-2}} \tag{18}$$

The nonuniform aperture phase distribution introduced by the feed displacement is responsible for the beam deviation, as already commented, but also leads to pattern deterioration, which includes beam broadening and null filling. These effects increase as δ_f becomes larger, resulting in substantial gain loss. Nevertheless, scanning of the beam by feed displacement is a technique widely used in practice, especially when it is difficult or impossible to move the reflector itself.

Summary of Parabolic Reflector Properties. There are a large number of possible reflector geometries, feed types, locations, and polarizations. Representative configurations were examined in the previous subsections to provide specific values as well as general conclusions. The many possible configurations employing a parabolic reflector are summarized in Table 3 together with XPOL, beam squint, and beam deviation effects. Table 3 shows that unbalanced feeds (i.e., the primary radiation pattern is not symmetric) usually generate substantial XPOL independent of the feed polarization or reflector configuration. Beam squint normally occurs with circularly polarized feeds, except for small reflector antennas (i.e., $D < 12\lambda$ and $F/D_p < 0.25$), where it can also be present with a linearly polarized illumination (21). Also, displacing the feed from the focal point normally generates XPOL and beam deviation. Table 3 presents a complete overview of the various depolarization and beam-pointing properties of single parabolic reflector antennas, which is of fundamental importance for designing effective reflector configurations.

Design of Axisymmetric and Offset Parabolic Reflector Antennas

Design of reflector antennas presents a challenge to the antenna engineer, especially in that so many parameters are available for adjustment. The main purpose of this subsection is to present a complete procedure to design axisymmetric and offset reflectors, as well as to provide some insights into the basic tradeoffs inherent in the process.

Table 3. Polarization and Beam Pointing Characteristics of Single Parabolic Reflectors

Reflector Geometry	Location	Feed Type	Polarization	Cross Polarization	Beam Squint
Axisymmetric	On Focus	Balance	Linear	No	No
			Circular	No	No
		Unbalanced	Linear	Yes	No
			Circular	Yes	No
	Off Focus[a]	Balanced	Linear	Yes	No
			Circular	Yes	Yes
		Unbalanced	Linear	Yes	No
			Circular	Yes	Yes
Offset ($\psi_f > 0°$)	On Focus	Balanced	Linear	Yes	No[b]
			Circular	No[b]	Yes
		Unbalanced	Linear	Yes	No[b]
			Circular	Yes	Yes
	Off Focus[a]	Balanced	Linear	Yes	No[b]
			Circular	Yes	Yes
		Unbalanced	Linear	Yes	No[b]
			Circular	Yes	Yes

[a] Beam deviation also occurs; see the subsection entitled "Beam Deviation."
[b] Except for small reflector antennas (i.e., $D < 12\lambda$ and $F/D_p < 0.25$); see Ref. 21 for further details.

Within this context, we start by examining the influence of the feed pointing angle ψ_f on the gain G, sidelobe level (SLL), and cross polarization of offset reflectors having $H > D/2$ (i.e., general offset reflectors). The feed pointing angle is a parameter of significant influence on the electrical behavior of reflector antennas and provides many insights into XPOL behavior. Scattering from supporting structure (struts) is not included, but for an offset configuration it is typically negligible. An offset reflector is chosen with a diameter $D = 85.5\lambda$, $F/D_p = 0.3$, and offset distance $H = 5D/8$, corresponding to a geometry that is popular in VSAT applications. The balanced feed pattern employed to illuminate the reflector is x_f-polarized, as modeled by Eqs. (14) and (15), with a 10 dB beamwidth of 70°.

Figure 9 shows the gain, SLL, and XPOL computed with GRASP (14) as the feed pointing angle, ψ_f, is varied for the selected configuration. We note that the gain curve has a broad peak, and the sidelobe level is not sensitive to feed pointing except at very small angles ($\psi_f < 30°$). Only the near-in sidelobes were considered in this analysis, and therefore spillover from the feed, which is particularly high for $\psi_f < 40°$ and $\psi_f > 60°$, was not included in Fig. 9. The XPOL, however, decreases with decreasing ψ_f. Although illustrated for a particular case example, this is a generic and important result, showing that in the limiting case where the feed is pointed at the apex of the parent paraboloid (i.e., $\psi_f = 0°$), negligible XPOL is generated (15). However, this leads to large spillover and associated gain loss. Therefore, in practice the feed is tilted to direct its pattern toward the reflector, which introduces high XPOL. For approximate designs, such as are often sufficient in practice, the feed can be aimed within the range $40° \leq \psi_f \leq 60°$ in order to keep spillover losses (and consequent gain loss) reasonable. For the particular configuration herein considered, peak gain operation is achieved with $\psi_f = 47°$, which yields $G = 47.52$ dBi.

A classical design scenario has now emerged. The feed pointing angle ψ_f is reduced until desirable cross-polarization performance is achieved or until the gain is reduced as far as can be accepted. If, on the other hand, the SLL is a critical parameter, ψ_f can be optimized to yield nearly the lowest SLL over a practical range of angles, with only small reductions in G and the XPOL (15). This is discussed in more detail in the procedure for designing parabolic antennas, presented next.

We now have a reasonable understanding of the basic concepts of reflector antennas. The following steps summarize a procedure to design axisymmetric and offset reflector antennas:

1. *Determination of Reflector Diameter.* The following equation is very useful to estimate a value of D to

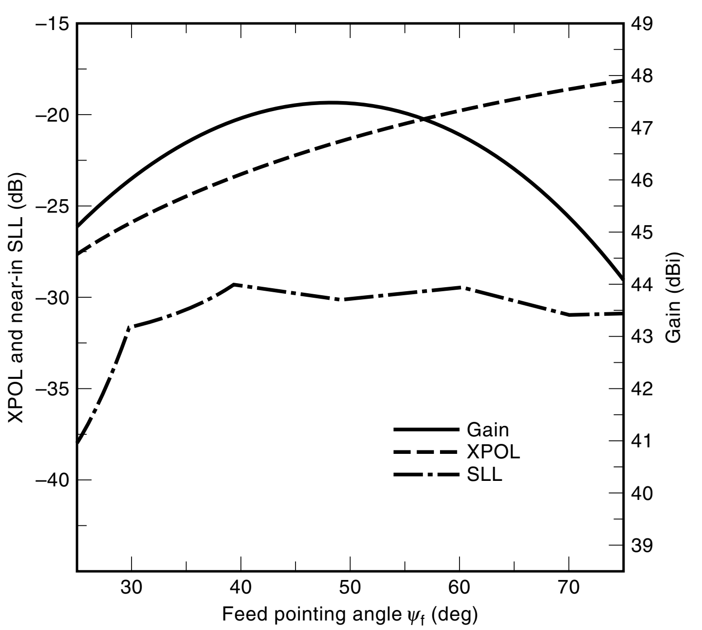

Figure 9. Gain, sidelobe level (SLL), and cross-polarization level (XPOL) as a function of the feed pointing angle ψ_f for an offset parabolic reflector with a 85.5λ diameter.

achieve a required gain G (20):

$$g_{[\text{not in dB}]} = \epsilon_{\text{ap}} \frac{4\pi A_{\text{p}}}{\lambda^2} = \epsilon_{\text{ap}} \left(\frac{\pi D}{\lambda}\right)^2 \tag{19}$$

where A_p is the physical area of the antenna aperture and ϵ_{ap} is the *aperture efficiency,* typically 0.65 (65%) for many parabolic reflector systems used in practice. Note that the gain in decibels is $G = 10 \log g$.

2. *Determination of Offset Distance.* The offset distance H controls the amount of blockage caused by the feed and supporting structure on the reflector projected aperture. Many reflectors nowadays are just fully offset paraboloids ($H = D/2$) (i.e., the bottom of the reflector just touches its axis of symmetry). This configuration avoids the blockage from the feed supporting structure (struts) and waveguide, although part of the feed aperture is still directly in front of the reflector. Nevertheless, the total blockage area is still significantly smaller than the one presented by axisymmetric configurations ($H = 0$). Values of H larger than $D/2$ can overcome blockage, but also increase the total volume occupied by the reflector, which in some cases is undesirable. In addition, the manufacturing process and associated adjustments become more difficult as H increases.
3. *Selection of Reflector Curvature.* Values usually encountered in practice for the reflector curvature, F/D_p, are between 0.25 and 1.0, where D_p is given by Eq. (13). Higher values ease the manufacturing process (i.e., the reflector is flatter) but require a narrower feed pattern to illuminate the reflector, which results in larger feed antennas. A typical value nowadays is $F/D_p = 0.3$, which yields a compact design.
4. *Determination of Feed Pattern.* An important parameter for determining the necessary feed pattern is the *reflector illumination* RI in the aperture plane, which, in decibels, is given by

$$\text{RI} = 20 \log \cos^2 \frac{\theta_{\text{f}} + \psi_{\text{f}}}{2} + 20 \log \cos^q \theta_{\text{f}} \tag{20}$$

where the first term in the right is normally referred to as *spherical spreading loss* and takes account of the power spreading due to spherical propagation of the wave between the focal point and the parabolic reflector surface. The second term in the right side of Eq. (20) is the normalized feed pattern in decibels of

$$C(\theta_{\text{f}}) = \cos^q \theta_{\text{f}} \tag{21}$$

which is a pattern model widely used in practice with Eq. (14), as an alternative to the one given by Eq. (15). The main advantage of Eq. (21) over Eq. (15) is that the directivity of the feed, or its gain if ohmic losses are not taken into account, can be found analytically in closed form with (4)

$$g_{\text{f}[\text{not in dB}]} = 4q + 2 \tag{22}$$

where g_f is the gain of the balanced feed modeled by Eqs. (14) and (21). The parameter q can be obtained from Eq. (20) for a required reflector illumination RI in decibels at a direction θ_f as

$$q = \frac{\dfrac{\text{RI}}{20} - \log \cos^2 \dfrac{\theta_{\text{f}} + \psi_{\text{f}}}{2}}{\log \cos \theta_{\text{f}}} \tag{23}$$

A usual value for RI at the reflector edges, often referred to as the *edge illumination* EI, is −11 dB and assures optimal gain performance for axisymmetric paraboloids ($\psi_f = 0°$ and $\theta_f = \psi_L = \psi_U$); see Ref. 20. In offset reflectors, $\psi_L \neq \psi_U$, but an specified value of EI at both edges can still be obtained by solving for ψ_f the equation formed by imposing that $q(\theta_f = \psi_L) = q(\theta_f = \psi_U)$. Once ψ_f is determined, the parameter q can be calculated directly from Eq. (23) for the specified value of RI (i.e., EI), at either $\theta_f = \psi_L$ or $\theta_f = \psi_U$, since they now should yield the same result. Under this condition, the edge illumination is called *balanced* and yields near-minimum sidelobe levels over practical ranges of feed pointing, with only small penalties in gain and XPOL (15). A graphical technique to determine ψ_f for the same condition was introduced in Ref. 15 and is especially indicated when only measured feed patterns are available. In practice, however, it is common to find offset systems employing $\psi_f = \psi_B$, Eq. (11), or $\psi_f = \psi_C$, Eq. (12). For either case the edge illumination is in general unbalanced. As a consequence, different values of q are obtained with Eq. (23), depending on whether $\theta_f = \psi_L$ or $\theta_f = \psi_U$. A simple arithmetic mean can then be taken to specify the required feed pattern. Although approximate, this simple procedure yields reasonably good results in practice and is well suited for our purposes. Once the parameter q is determined, Eqs. (22) and (19) can be used to estimate the aperture diameter, or area, of the required feed antenna. A typical value of $\epsilon_{ap} = 0.55$ (55%) can be used for feed horns. A more exact approach is available when the feed antenna is an open-ended rectangular waveguide of wide and narrow dimensions a and b, or an open-ended circular waveguide of radius a. For those cases, the waveguide dimensions can be determined from Eq. (22) with $g_f = 32ab/\pi\lambda^2$ ($\epsilon_{ap} \approx 0.81$) or $g_f = 10.5\pi a^2/\lambda^2$ ($\epsilon_{ap} \approx 0.84$). If the result indicates a feed antenna with an aperture considered too large, a higher value of RI (i.e., EI at the reflector edges) should be employed to avoid unnecessary blockage. For an offset reflector, a larger value of H can also be tried and the whole procedure needs to be repeated.

The aforementioned design procedure was successfully employed to obtain the preliminary design of a 1.6 m just fully offset paraboloid, built and tested at the University of Brasilia for satellite TV reception at C band (Fig. 10). Nevertheless, the use of a suitable computer code before the manufacturing process is highly recommended to confirm the electrical performance of the reflector system. Techniques often implemented in numerical codes for the analysis of reflector antennas are discussed in the section entitled "Analysis Methods and Evaluation."

As a final note, we mention that surface distortions from ideal parabolic shapes are normally introduced in any manufacturing process. Random reflector surface errors can be al-

Figure 10. Just fully offset parabolic reflector antenna for satellite TV reception at C band, built and tested at the University of Brasilia. (Courtesy of Carlos Muller, University of Brasilia.)

lowed for by augmenting the aperture efficiency in Eq. (19) to include a *random surface error efficiency,* ϵ_{rs} (20):

$$g_{[\text{not in dB}]} = \epsilon'_{ap}\epsilon_{rs}\left(\frac{\pi D}{\lambda}\right)^2 \tag{24}$$

where

$$\epsilon_{rs} = e^{-(2\beta\delta_S)^2} \tag{25}$$

The parameter δ_S is the root mean square (rms) surface deviation and is approximately one-third of the peak-to-peak error (20). Detailed information on other efficiency factors left in ϵ'_{ap} can be found in the literature (20). Mass production of reflectors using presses and molds to shape glass fibers and other components normally yields $\delta_S \approx 0.01\lambda$ ($\epsilon_{rs} = 0.98$ or 98%). Errors larger than that can cause significant gain loss and pattern deterioration due to the introduction of phase errors. Machined metal reflectors are very accurate and have $\delta_S \approx 0.04$ mm. Reflector antennas are wideband devices by nature and are limited at the upper frequencies by the smoothness of the reflector surface and at the lower ones by the reflector electrical size. The operating bandwidth of a reflector antenna in practice is normally set by the bandwidth of the feed antenna employed to illuminate the reflector. Although herein illustrated for parabolic reflectors, random surface errors occur in any type of reflector antenna, such as the ones discussed next.

Other Single-Reflector Systems

A few other types of parabolic reflectors can also be obtained from Fig. 4, including offset configurations. The *parabolic cylinder,* for example, is generated by displacing the parabolic curve along the y axis. This yields a focal line in contrast to the focal point of the parabolic reflector. A feed line or a linear array of feed antennas must be placed along the focal line for proper illumination of the reflector. Another example is the *parabolic torus,* formed by rotating the parabolic curve with respect to an axis perpendicular to the s axis of Fig. 4. The axis of revolution is, in general, placed at a distance from the apex greater than F and is confined to the plane shown by Fig. 4. Thus the parabolic torus possesses a focal arc and can be visualized as a curved parabolic cylinder. Multiple feeds are normally employed to illuminate different sections of the reflector, producing independent beams with a single reflector antenna, a configuration widely used in satellite communications.

An example of a reflector antenna not generated by a parabolic curve is the spherical reflector, which is a section of a sphere. The Arecibo Observatory, located in Puerto Rico, employs an axisymmetric spherical main reflector with a diameter of 305 m for radio astronomy, ionospheric research, and radar investigation of celestial bodies. A line feed is used because parallel rays coming from space are reflected along the reflector axis (22). This is in contrast to the parabolic cylinder, where the focal line is perpendicular to the reflector axis of symmetry. However, the spherical reflector does not merely possess a focal line, but rather a focal region where feeds can be placed (23). Dual-offset shaped reflectors have also been proposed and used as feed systems in order to correct the nonuniform phase distribution characteristic of spherical reflectors (22). Dual- and multiple-reflector systems are treated in the next section.

MULTIPLE-REFLECTOR ANTENNA SYSTEMS

Cassegrain, Gregorian, and Multiple-Reflector Systems

Dual-reflector systems, such as the ones in Fig. 2(b, d), can be formed by adding to the parabolic reflectors previously studied a hyperbolic reflector (Cassegrain system) or an elliptical reflector (Gregorian system). Hyperbolic and elliptical reflectors have two focal points, F_1 and F_2, and are normally referred to as subreflectors because they are smaller than the parabolic main reflector.

It is known (3,24) that any ray coming from one of the focal points, say F_2, is reflected by an ellipsoid surface toward the other focal point, F_1. For the hyperbolic surface, the reflection occurs such that the reflected ray appears to come from F_1. Thus, any circular cone of rays (i.e., a section of a spherical wave) emanating from F_2 and directed to an elliptical, or hyperbolic, subreflector will then be reflected as another circular cone of rays with vertex at the other focal point F_1. Furthermore, if F_1 is coincident with the paraboloid focal point F, and the feed is located at F_2, a perfect circular cone of rays originated at F_1 will illuminate the paraboloid. Due to the paraboloid's reflecting property, a section of a plane wave will then appear at the paraboloid aperture plane.

There are a few basic advantages of dual configurations over single ones. They provide a shorter waveguide run to the feed antenna. In addition, dual configurations present lower noise when used as satellite earth terminals. This is due to the limited noise introduced by the feed spillover beyond the subreflector, given that it is now directed to cold sky, rather than hot earth as in the single-reflector case. Many satellite communication networks employ dual configurations as earth terminal antennas. Finally, the inclusion of the subreflector introduces another degree of freedom, which can be used to enhance electrical performance, such as by canceling XPOL in offset systems and/or prescribing the main aperture amplitude and phase distributions in dual shaped reflectors.

Within this context, dual shaped reflectors can be used to illuminate larger reflectors, such as the Arecibo spherical reflector (22), forming a multiple-reflector system. In this case, they are shaped to correct the phase aberration characteristic of spherical reflectors. They can also be used to enhance the scanning properties of spherical reflectors (25).

A multiple-reflector system can also be formed with a parabolic main reflector, which is illuminated by a sequence of hyperboloids and/or ellipsoids employed as subreflectors. The subreflectors must be properly arranged so that a spherical wave is formed after each reflection. It can be shown (26) that such a multiple-reflector system is always equivalent to a single parabolic reflector, normally referred to as the *equivalent paraboloid.* This concept also applies to Cassegrain and Gregorian systems (24,26), and is especially useful to determine the conditions for canceling XPOL in offset systems, as discussed next.

Conditions for Minimizing Cross Polarization in Offset Cassegrain and Gregorian Systems

The Cassegrain and Gregorian offset configurations of Fig. 2(d) can be optimized to cancel reflector-induced XPOL. We focus our discussion on the Gregorian system, but all main results herein presented are also valid for the Cassegrain system (3,23–24). Although less compact, the Gregorian configuration has been increasily used in practical applications, especially due to the fact that it allows the main reflector to have a just fully offset geometry (i.e., the bottom of the main reflector just touches its axis of symmetry). Cost-effective designs often require that an existing single-offset reflector mold be used to construct the main reflector of a dual configuration. However, many such existing molds in industry are for just fully offset geometries, which justifies the recent preference for Gregorian configurations. [To upgrade an existing mold to a dual-offset Cassegrain system, a main reflector other than just fully offset is normally required to avoid blockage, because the hyperbolic subreflector, in contrast to the elliptical one, is located above the axis of symmetry of the parent main reflector, as shown by Fig. 2(d).] In addition, the Gregorian configuration allows the main reflector also to be used as a single focused configuration without the need of removing the subreflector; see the next subsection for further details. Nevertheless, Cassegrain configurations have also been widely used in many practical systems, and all conditions for minimizing XPOL herein discussed also apply to them.

The general geometry of a dual offset Gregorian configuration is shown in Fig. 11, and the symbols are defined in Table 4. Although not shown in Fig. 11, the main reflector projected aperture is circular, such as the one in Fig. 4. The subreflector employed in a Gregorian offset design is a section of a parent ellipsoid described by the following expression:

$$\frac{(x_S - c)^2}{(f_S + c)^2} + \frac{y_S^2 + z_S^2}{(f_S + c)^2 - c^2} = 1 \tag{26}$$

where all variables and coordinates are as defined in Fig. 11 and Table 4. It is worth mentioning that the projections of the subreflector onto the $y_S z_S$ and $x_S y_S$ planes are ellipses.

As mentioned in the previous subsection, the geometry of Fig. 11 is equivalent to a single parabolic system. Furthermore, we saw previously that if the feed pointing angle ψ_f is coincident with the reflector axis of symmetry, no substantial XPOL is generated. This condition can be satisfied for the equivalent single paraboloid, provided that the original dual

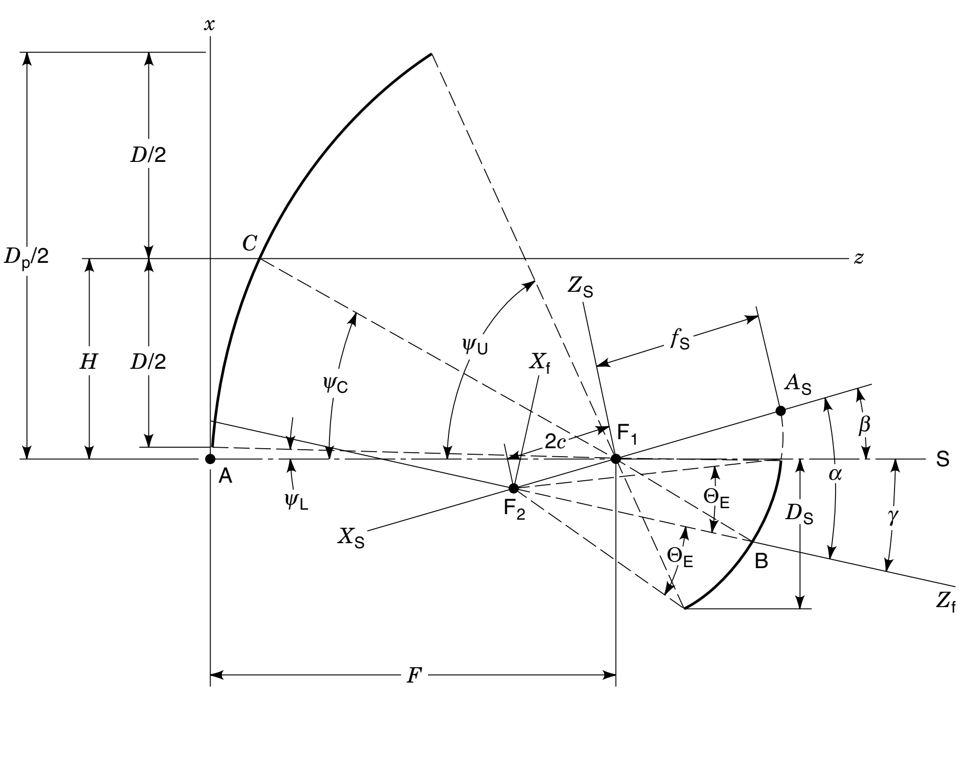

Figure 11. General geometry of the dual offset Gregorian reflector antenna. The symbols are defined in Table 4.

Table 4. Definitions of Symbols for Dual Configuration

Symbol	Definition
D	Diameter of the projected aperture of the parabolic main reflector
D_p	Diameter of the projected aperture of the parent paraboloid
H	Offset of reflector center
F	Paraboloid focal length
Point F_1	Common focal point of the parabolic main reflector and ellipsoidal subreflector
Point F_2	Ellipsoid focal point; feed antenna location
Point A	Apex of the parent paraboloid
Point A_S	Apex of the ellipsoidal subreflector
Point B	Point on subreflector that bisects subtended angle viewed from F_2. Point B also results from the intersection of the ray coming from point C on the main reflector and the feed axis (z_f)
Point C	Point on main reflector that projects to the center of the circular projected aperture
ψ_C	Angle of feed antenna pattern peak after reflecting on the subreflector relative to the main reflector axis of symmetry (s)
$\psi_U - \psi_L$	Angle subtended by the parabolic main reflector as viewed from the focal point F_1
D_S	Height of the ellipsoidal subreflector
e	Subreflector eccentricity ($0 < e < 1$ for an ellipsoid)
c	Half of the ellipsoid interfocal distance
F_S	Distance between a focal point and the closest ellipsoid apex
α	Feed pointing angle measured relative to the ellipsoid axis of symmetry (x_s)
β	Angle between the ellipsoid and parent paraboloid axes of symmetry (x_S and s, respectively)
γ	Angle between the main reflector and feed axes (s and z_f)
θ_E	Half the angle subtended by the subreflector as viewed from the feed antenna location (ellipsoid focal point F_2)

configuration of Fig. 11 satisfies the following relation (27):

$$\tan\alpha = \frac{|e^2 - 1|\sin\beta}{(1 + e^2)\cos\beta - 2e} \tag{27}$$

where e is the subreflector eccentricity ($0 < e < 1$ for an ellipsoid and $e > 1$ for a hyperboloid), $e = c/(f_S + c)$. Equation (27) is generally referred to as the *Mizugutch condition* and has the following alternative form, known as the *Dragone condition* (24,26):

$$\tan\frac{\alpha}{2} = \frac{e + 1}{|e - 1|}\tan\frac{\beta}{2} \tag{28}$$

where the factor $(e + 1)/(|e - 1|)$ is normally referred to as the *subreflector magnification M.* Rusch (24) gave a condition based on the same equivalent-paraboloid concept that simultaneously minimizes XPOL and spillover loss (i.e., feed radiation missing the subreflector):

$$\tan\frac{\beta}{2} = \left(\frac{e - 1}{e + 1}\right)^2 \tan\frac{\beta + \psi_C}{2} \tag{29}$$

where ψ_C is the angle subtended to the center of the main reflector and is given by Eq. (12). The *Rusch condition,* Eq. (29), can only be applied to dual systems employing a parabolic main reflector with a circular projected aperture, in contrast to the Mizugutch and Dragone conditions, Eqs. (27) and (28), which can be applied to reduce XPOL in systems with arbitrary projected apertures. Although more restrictive, the Rusch condition, in addition to XPOL, also minimizes spillover loss, given that the resulting equivalent paraboloid is constrained to be always axisymmetric (24). This yields the feed axis of the original dual configuration pointing in the direction that bisects the subreflector subtended angle, as shown in Fig. 11. Enforcement of Mizugutch or Dragone conditions, in general, does not result on an axisymmetric equivalent paraboloid, which leads to high spillover loss even though XPOL is kept to a minimum. In fact, the result in the Rusch condition, Eq. (29), can be visualized as the one particular solution of Eq. (27) or (28) that yields an axisymmetric equivalent paraboloid with $\psi_f = 0°$, thus simultaneously minimizing XPOL and spillover loss.

It is important to note that Eqs. (27) to (29) are effective only in reducing the reflector-induced XPOL. A simple worst-case model for predicting the influence of feed XPOL in reflector systems is (18)

$$\mathrm{XPOL_S} = \mathrm{XPOL_F} + \mathrm{XPOL_R} \tag{30}$$

where $\mathrm{XPOL_S}$, $\mathrm{XPOL_F}$, and $\mathrm{XPOL_R}$, are, respectively, the cross-polarization levels of the total system, the feed, and the reflector(s). The XPOL here is expressed as a field ratio (not in decibels; it is $10^{(\text{value in dB})/20}$). The simple result in Eq. (30) shows that either the feed or the reflector XPOL can dominate the system XPOL. Since dual offset configurations satisfying any of the conditions in Eqs. (27) to (29) yield low reflector XPOL, system XPOL is usually limited by feed XPOL. We use, as an example, a low-cross-polarization dual offset Gregorian reflector antenna, employing a just fully parabolic main reflector with a 2.4 m diameter. When a feed XPOL value of −32 dB is included, the system XPOL computed by GRASP (14) increases from −48.19 dB to −31.75 dB. Equation (30) yields −30.75 dB, which is in good agreement for such a simple formula. In addition, Eq. (30) can be used to predict a feed XPOL level required to attend a given specification of system XPOL.

As an illustration of using the minimum XPOL conditions expressed in Eqs. (27) to (29), we consider the following offset parabolic system.

The Green Bank Radio Telescope

The Green Bank Radio Telescope (GBT) will be the largest fully steerable radio telescope in the world. It is currently under construction (as of January 1998) and is expected to be completed by 1999 (Figs. 12 and 13). Its offset design provides a clear 100 m diameter projected circular aperture. The GBT structure can be pointed to view the entire sky down to a 5°

Figure 12. Construction site of the Green Bank Radio Telescope reflector antenna. The 100 m main reflector consists of 2000 solid panels. The structure can be pointed to view the entire sky down to a 5° elevation angle and will be the largest fully steerable radio telescope in the world. (Courtesy of George Behrens, National Radio Astronomy Observatory.)

elevation angle, using a wheel-and-track mechanical design. The reflecting surface consists of 2000 solid panels that can be positioned using actuators behind the panels. A laser ranging system will be used to determine the positions of the panels, adjusting the surface accuracy with closed-loop control.

The GBT is connected to radiometers that can receive signals in several frequency bands. From 290 MHz to 1230 MHz, the GBT operates as a single offset reflector using a feed assembly aimed directly at the main reflector. From 1 GHz to 45 GHz, it operates as a Gregorian dual offset reflector using the feeds in the receiver room that are aimed at the ellipsoidal subreflector. The Gregorian configuration has the focal points in the area between the subreflector and the main reflector, allowing the subreflector to remain fixed even when the telescope operates in the single-offset-reflector mode. This is not possible with a Cassegrain configuration (28).

We start by examining the GBT single-offset configuration, with the characteristics listed in Table 5, employing the codes

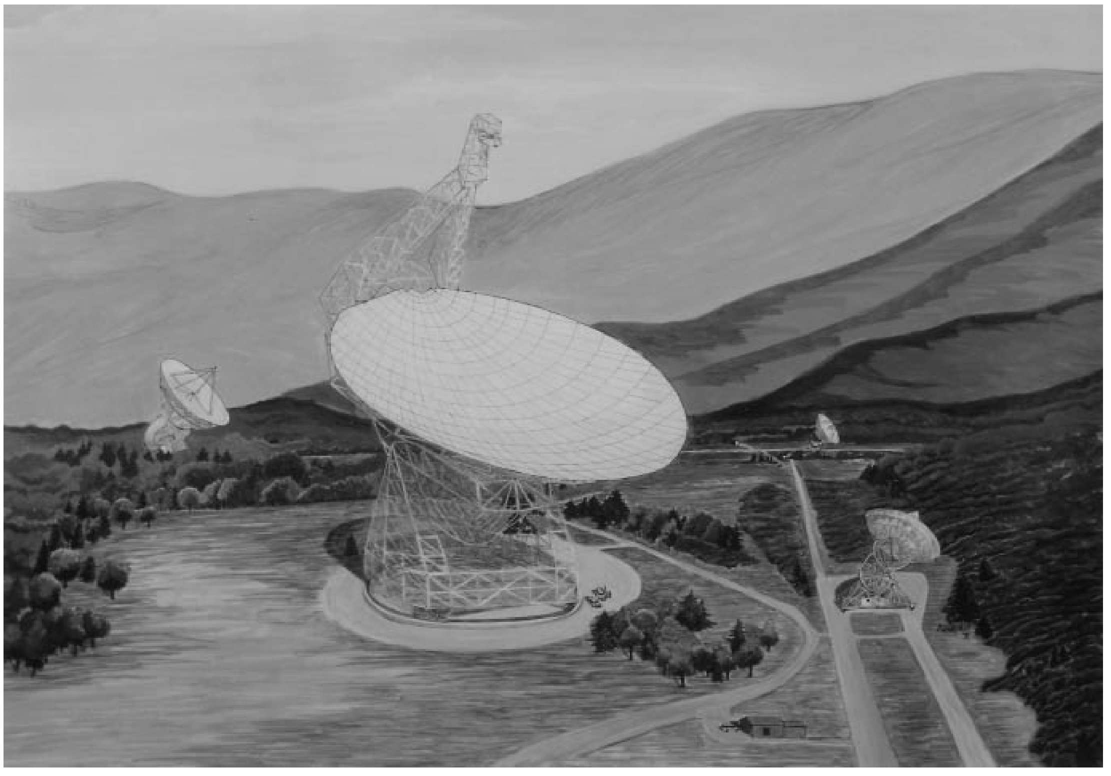

Figure 13. Artwork of the Green Bank Radio Telescope reflector antenna. The dual offset Gregorian configuration employs an offset parabolic main reflector with a 100 m projected aperture diameter. (Courtesy of George Behrens, National Radio Astronomy Observatory.)

Table 5. GBT Single Offset Reflector Configuration and Computed Performance Values

Main Reflector Configuration		
Shape:		Offset parabolic
Projected diameter D (m):		100
Parent ref. diameter D_p (m):		208
Focal length F (m):		60
Offset of reflector center, H (m):		54
Computation:	PRAC	GRASP
Feed Configuration (On Focus)		
Polarization:	Linear (x_f)	Linear (x_f)
Pattern shape:	$\cos^{4.58}$; Eqs. (14) and (21)	Gaussian; Eqs. (14) and (15)
Gain G_f (dBi):	13.08	13.14
10 dB beamwidth (deg):	77.92	77.92
Feed angle ψ_f (deg):	42.77	42.77
System Performance		
Gain G (dBi)	82.87	82.79
Cross-polarization level, XPOL (dB):	−21.54	−21.56
Sidelobe level, SLL (dB)	−26.72	−27.21
Aperture efficiency ϵ_{ap}, %	78.48	77.05

GRASP (14) and PRAC (7). Further information on PRAC (parabolic reflector analysis code) is presented in the section entitled "Numerical Implementation and Accuracy Evaluation." The performance values, also listed in Table 5, were computed at 15 GHz in the plane normal to the plane of symmetry (i.e., the *yz* plane of Fig. 4). Note that the two codes yield very similar results for this geometry. We note from Table 5 that the gain is 82.87 dBi and the XPOL is −21.54 dB (61.33 dBi), as computed by PRAC.

To lower the XPOL, we upgrade the GBT single-offset system of Table 5 to a low-cross-polarization dual-offset Gregorian antenna according to Eq. (29). Design parameters, such as the desired subreflector size, were obtained from Ref. 28. The resulting configuration is listed in Table 6 and agrees with Ref. 28. New dual configurations employing the same GBT offset main reflector of Table 5 can be obtained using different design parameters, such as a new subreflector size or feed configuration, as discussed in Ref. 29.

Table 6 also presents the performance values at 15 GHz computed with GRASP in the same plane considered for the single-offset configuration previously discussed. We note that the XPOL is now −43.01 dB, more than 20 dB lower than the XPOL of the single configuration in Table 5. However, a feed antenna with high XPOL will likely degrade the total system XPOL performance, as addressed in the previous subsection.

ANALYSIS METHODS AND EVALUATION

Geometrical and Physical Optics Formulations

In both the geometrical optics (GO) and physical optics (PO) formulations, the ultimate goal is to determine equivalent currents, which can then be integrated to obtain the far-field patterns, a process well described in the literature on aperture antennas (20). We focus our attention on the assumptions and approximations inherent in each of these formulations, as well as on their intrinsic differences.

The GO technique yields the aperture fields, assuming equal angles of incidence and reflection. The far-field patterns can then be calculated using a Fourier transformation directly, which is equivalent to obtaining equivalent currents and then integrating, as described later in this subsection. With the use of image theory, it is necessary to know only the electric field distribution over the reflector projected aperture, $\boldsymbol{E}_r$, which is computed from the incident electric field $\boldsymbol{E}_i$ (i.e., the feed radiation), with (20)

$$\boldsymbol{E}_r = 2(\hat{\boldsymbol{n}} \cdot \boldsymbol{E}_i)\hat{\boldsymbol{n}} - \boldsymbol{E}_i \tag{31}$$

where $\hat{\boldsymbol{n}}$ is the unit vector normal to the surface; see Eq. (5). Equation (31) assumes that at the point of reflection the reflector is planar and perfectly conducting. In addition, the incident wave from the feed antenna is treated locally as a plane wave. These same assumptions are also used by the PO technique to determine the surface currents, $\boldsymbol{J}_s$, over the reflector as follows:

$$\boldsymbol{J}_s = 2\hat{\boldsymbol{n}} \times \boldsymbol{H}_i \tag{32}$$

where $\boldsymbol{H}_i$ is the incident magnetic field from the feed antenna and can be computed from Eq. (14), recalling that in the far field $\boldsymbol{H} = (\hat{\boldsymbol{r}} \times \boldsymbol{E})/\eta$ (where η is the free-space characteristic impedance). The PO approximation assumes that currents exist only over the side of the reflector directly illuminated by the feed antenna.

Table 6. GBT Dual Offset Reflector Configuration and Computed Performance Values

Main Reflector Configuration

Shape: Offset paraboloid
Projected diameter D: 100 m
Parent reference diameter D_p: 208 m
Focal length F: 60 m
Offset of reflector center, H: 54 m
Angle β, 5.58°

Subreflector Configuration

Shape: Offset ellipsoid
Projected height D_S: 7.55 m
Parameter c of ellipse: 5.9855 m
Parameter f_S of ellipse: 5.3542 m
Eccentricity e: 0.5278

Feed Configuration (On Focus; GRASP Calculation)

Polarization: Linear (x_f)
Pattern shape: Gaussian, Eqs. (14) and (15)
Gain G_f: 21.31 dBi
10 dB beamwidth: 30°
Angle α: 17.91°
Angle γ: 12.33°

System Performance (GRASP Calculation)

Gain G: 82.83 dBi
Cross-polarization (XPOL) level: −43.01 dB
Sidelobe level (SLL): −22.56 dB
Aperture efficiency ϵ_{ap}: 77.76%

The far-field pattern can then be determined by summing the individual contributions of each current point over the surface, taking into account the different amplitudes and phases due to the excitation and spatial location. Antenna theory shows that a unit point source of current radiates a spherical wave, which is normally referred to as the free-space *Green's function* ($e^{-jkr}/4\pi r$); see Ref. 20 for further details. In the limit as the current distribution becomes continuous, such as the one given by Eq. (32), the weighted sum of spherical waves becomes an integral, yielding the radiated patterns.

Note that the integration process for obtaining the patterns is the same as the one employed by the GO technique, given that once the aperture distribution is determined from Eq. (31), equivalent currents can then be obtained and integrated over the reflector aperture. This process is equivalent to computing the Fourier transform of the aperture distribution given in Eq. (31). One difference between GO and PO is that PO currents are determined over the reflector *curved* surface and the GO equivalent currents over the *planar* projected aperture, with the latter already in a format more appropriate for integration through a Fourier transform. However, the use of a Jacobian transformation (3,4) maps the PO currents over the reflector curved surface to the planar aperture, yielding the possibility of also using Fourier transformations for performing the integration. Analytical integration is only possible for symmetrical reflectors (4,8), and numerical techniques are normally required to evaluate offset reflectors, as discussed in the next subsection.

The PO formulation is generally considered more accurate than GO to evaluate offset reflectors, especially if XPOL assessment is a main concern. However, pattern accuracy as determined from both techniques degrades beyond the main beam and near-in sidelobes. The pattern in the far-out region is dominated by diffraction effects, especially scattering from the reflector and/or subreflector edges. This is taken into account by augmenting GO with the geometrical theory of diffraction (GTD) or augmenting PO with edge currents through the physical theory of diffraction (PTD); see Refs. 20 and 30 for details. However, the near-in pattern region is, most of the time, the region of interest when analyzing high-gain antennas such as the reflector antennas considered here.

Numerical Implementation and Accuracy Evaluation

In this subsection we discuss one of many possible numerical implementations of the PO formulation previously addressed; see Ref. 4 for alternative procedures. Reflector surface currents are computed from Eq. (32) for the balanced feed model given by Eqs. (14) and (21). A set of coordinate transformations, rotations, and translations, is necessary in order to describe the far-field patterns as a function of the reflector local coordinate system $\{xyz\}$, given that the feed pattern is described as a function of the feed local coordinate system $\{x_f y_f z_f\}$. Although not shown, Eulerian angles (31) are employed for generality, and we mention that a solid background in geometry and vector calculus is normally required for the analysis of reflector antennas.

The procedure employs a Jacobian transformation, as discussed in the preceding subsection, and evaluates numerically the following integral (4) using a numerical procedure based on the Gauss–Zirnike integration method (32):

$$\boldsymbol{E}(\boldsymbol{r}) = -j\frac{\eta}{2\lambda}\frac{e^{-jkR}}{R}(\boldsymbol{I} - \hat{\boldsymbol{r}}\hat{\boldsymbol{r}}) \cdot \iint_{s'} \boldsymbol{J}(\boldsymbol{r}')J_{\Sigma}e^{jk\hat{\boldsymbol{r}}\cdot\boldsymbol{r}'}\,ds' \qquad (33)$$

where $\hat{\boldsymbol{r}}\hat{\boldsymbol{r}} \cdot \boldsymbol{a}$ is shorthand for $\hat{\boldsymbol{r}}(\hat{\boldsymbol{r}} \cdot \boldsymbol{a})$, and $\boldsymbol{I} - \hat{\boldsymbol{r}}\hat{\boldsymbol{r}}$ is included to remove the radial component (far-field approximation) (4). The unit dyad $\boldsymbol{I}$ is equal to the identity matrix for our purposes, and the Jacobian transformation J_{Σ} (4,31) is employed to allow the integral to be evaluated over the reflector planar projected aperture s'. However, the currents are still defined over the reflector curved surface. In addition, the Jacobi–Bessel method (31) is used to express part of the kernel in Eq. (33) as a sum over a set of orthogonal functions defined on the antenna aperture. Within this context, numerical integration is necessary only to evaluate the coefficients of the series expansion, which employs the modified Jacobi polynomials in the radial direction and a Fourier series in the circumferential direction.

The aforementioned procedure was implemented in the code PRAC (7). PRAC is a user-friendly code developed by the author to analyze axisymmetric and offset parabolic reflectors, and it yields the co- and cross-polarized radiated fields with high accuracy and efficiency. PRAC is currently being used by many universities and major industries worldwide, and a freeware version of the code is expected to be distributed with the electronic version of this encyclopedia.

To evaluate the accuracy of the code, we select as a baseline configuration for analysis a just fully offset paraboloid with a diameter $D = 85.5\lambda$, $F/D_p = 0.3$, and offset distance $H = 42.75\lambda$. The reflector illumination is modeled by the balanced feed described by Eqs. (14) and (21), with a 10 dB beamwidth of 78° ($q = 4.57$ yielding a feed gain of 13.07 dBi). The offset reflector choice corresponds to a 1.8 m diameter VSAT earth terminal antenna operating at 14.25 GHz, similar to the one shown in Fig. 14.

Figure 15 shows the computed co- and cross-polarized patterns and measured data for the example offset parabolic reflector in the plane normal to the plane of symmetry (i.e., the *yz* plane). The XPOL is expected to be maximum at this plane, as discussed in the subsection titled "Cross Polarization." We note from Fig. 15 that the results obtained with PRAC are in good agreement with the measured data. The measured gain of 46.78 dBi is about 0.8 dB below the computed gain of 47.60 dBi due to losses and system imbalances. The system XPOL is also a little overestimated by the computer simulations for this example. In fact, the measured system XPOL is −22.00 dB, whereas PRAC yields −21.27 dB. Nevertheless, PRAC yields a valuable estimate on how the reflector system behaves electrically, showing the necessity of a numerical evaluation previous to the manufacturing process. It is worth mentioning that analysis of this same baseline configuration with the physical optics portion of GRASP (14) yielded almost identical results (7), with the exact same locations for the nulls and peak sidelobes and XPOL lobes, confirming the accuracy of PRAC and PO analysis for evaluating offset reflectors.

As final notes on the analysis of reflector antennas, we mention that the lower integration limit in Eq. (33) can be set so as to allow for a circular area of blockage equivalent to that normally caused by the feed and supporting structure in axisymmetric reflectors. In addition, the integral in Eq. (33)

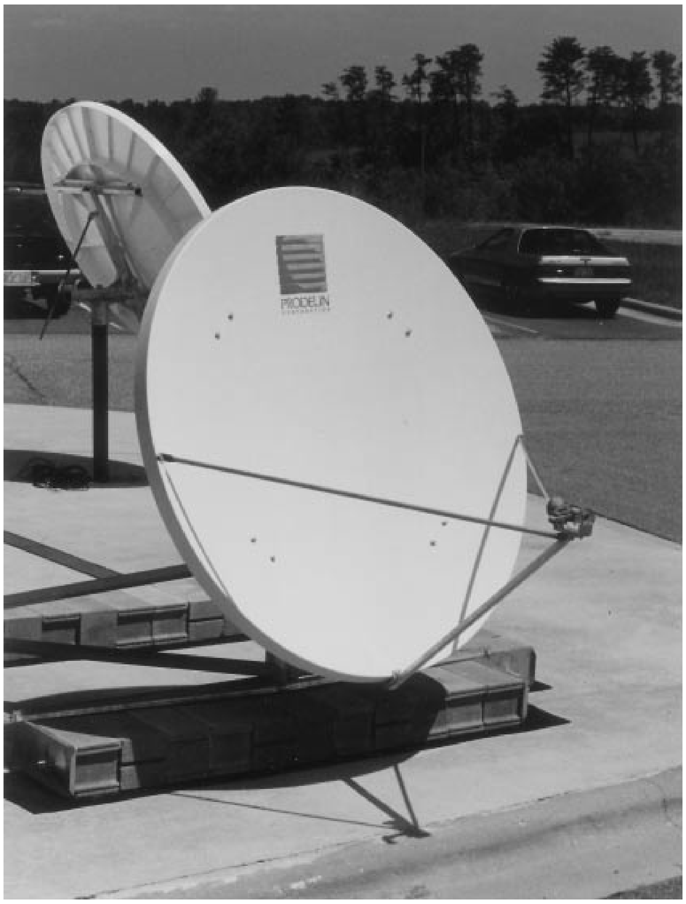

Figure 14. Just fully offset parabolic reflector antenna with a projected aperture diameter of 1.8 m. (Courtesy of Nick Moldovan, Prodelin Corporation.)

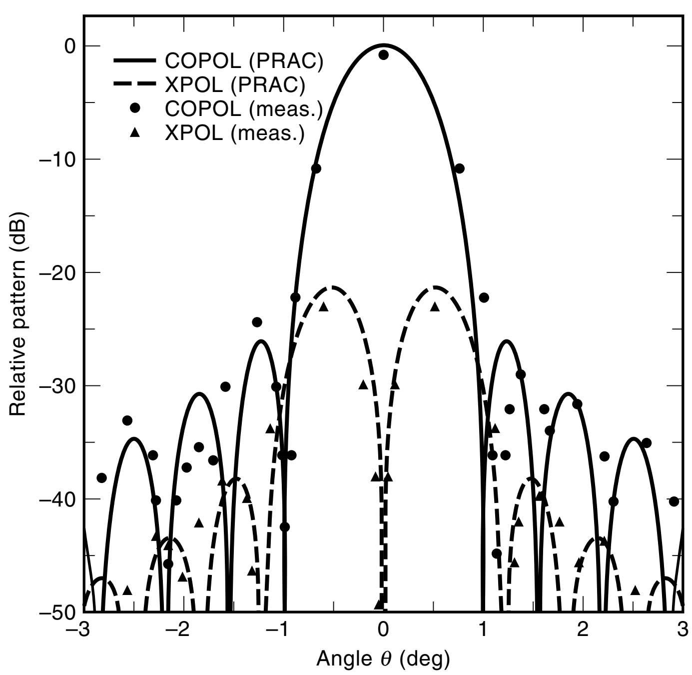

Figure 15. Computed and measured radiation patterns at 14.25 GHz of a 1.8 m single offset parabolic reflector antenna.

can also be evaluated over areas s' other than the circular, in order to analyze reflectors with projected apertures such as the elliptical one. Reflectors with elliptical apertures present a far-field pattern with a main beam that is narrower in the plane containing the major axis of the ellipse and are used in practice to transmit signals to synchronous satellites. The main advantage is a more compact design than for the full circular aperture, offering less resistance to wind and saving material during manufacture. The lower gain (i.e., wider beam) in the plane containing the minor axis of the ellipse does not degrade system performance for this particular application, given that only a single belt of synchronous satellites exists and therefore beam resolution is required only in one plane. Finally, both GO and PO formulations can also be used to evaluate dual and multiple-reflector systems. The simplest procedure is first to determine the radiation pattern of the system formed by the feed antenna and subreflector, and then to use this result as the incident field on the next subreflector or main reflector. It is also common to employ GO for the subreflector analysis and then PO in the final step to evaluate the main reflector for better accuracy. This combination saves computer time, as GO analysis is generally faster than PO (20).

FEED ANTENNAS

We start by discussing analytical models that approximately describe the electrical behavior of feed antennas usually encountered in practice. The simplest model is the balanced feed given by Eq. (14), normally used with Eq. (15) or (21). Balanced radiation patterns can be obtained in practice with the use of multimode horns, such as the Potter horn, and hybrid-mode horns, such as the conical corrugated ones (23,33). An alternative version of Eq. (14) can be obtained for feeds presenting different pattern cuts in the E-plane ($\phi_f = 0°$) and H-plane ($\phi_f = 90°$). The feed patterns in these two planes are, most of the time, all that is known. As in Eq. (14), we assume that the feed is purely linearly polarized in the x_f direction, yielding (3)

$$\boldsymbol{E}_f = \frac{e^{-jk\boldsymbol{r}_f}}{\boldsymbol{r}_f}[\hat{\boldsymbol{\theta}}_f C_E(\theta_f)\cos\phi_f - \hat{\boldsymbol{\phi}}_f C_H(\theta_f)\sin\phi_f] \tag{34}$$

where $C_E(\theta_f)$ and $C_H(\theta_f)$ denote the feed-pattern cuts in the E- and H-planes, respectively. A y_f-polarized feed pattern, as well as circularly polarized ones, can be obtained from Eq. (34) by introducing the modifications already suggested in the subsection entitled “Cross Polarization.” Note that Eq. (34) reduces to Eq. (14) for $C_E(\theta_f) = C_H(\theta_f) = C(\theta_f)$.

Finally, we can approximate even further the electrical behavior of feed antennas, although still ideally modeled with a fixed phase center, using the *complex polarization ratio* p_r, defined as

$$p_r = \mathrm{XPOL_F}(\cos\tau + j\sin\tau) \tag{35}$$

The quantity $\mathrm{XPOL_F}$ (not in decibels) determines the feed XPOL peak relative to the peak copolarized beam, and τ is the difference in phase between the cross- and copolarized feed patterns defined as

$$\tau = \mathrm{phase(XPOL_F)} - \mathrm{phase(COPOL_F)} \tag{36}$$

The final result, assuming a linear polarization in the x_{f} direction, is

$$\begin{aligned}\boldsymbol{E}_{\mathrm{CO}}(\boldsymbol{r}_{\mathrm{f}}) = \{&[C_{\mathrm{E}}(\theta_{\mathrm{f}})\cos^2\phi_{\mathrm{f}} + C_{\mathrm{H}}(\theta_{\mathrm{f}})\sin^2\phi_{\mathrm{f}}] \\ &+ p_{\mathrm{r}}[C_{\mathrm{E}}(\theta_{\mathrm{f}}) - C_{\mathrm{H}}(\theta_{\mathrm{f}})]\cos\phi_{\mathrm{f}}\sin\phi_{\mathrm{f}}\} \\ &(\hat{\boldsymbol{\theta}}_{\mathrm{f}}\cos\phi_{\mathrm{f}} - \hat{\boldsymbol{\phi}}_{\mathrm{f}}\sin\phi_{\mathrm{f}})\frac{e^{-jkr_{\mathrm{f}}}}{r_{\mathrm{f}}}\end{aligned} \tag{37}$$

and

$$\begin{aligned}\boldsymbol{E}_{\mathrm{CROSS}}(\boldsymbol{r}_{\mathrm{f}}) = \{&[C_{\mathrm{E}}(\theta_{\mathrm{f}})\sin^2\phi_{\mathrm{f}} + C_{\mathrm{H}}(\theta_{\mathrm{f}})\cos^2\phi_{\mathrm{f}}]p_{\mathrm{r}} \\ &+ [C_{\mathrm{E}}(\theta_{\mathrm{f}}) - C_{\mathrm{H}}(\theta_{\mathrm{f}})]\cos\phi_{\mathrm{f}}\sin\phi_{\mathrm{f}}\} \\ &(\hat{\boldsymbol{\theta}}_{\mathrm{f}}\sin\phi_{\mathrm{f}} - \hat{\boldsymbol{\phi}}_{\mathrm{f}}\cos\phi_{\mathrm{f}})\frac{e^{-jkr_{\mathrm{f}}}}{r_{\mathrm{f}}}\end{aligned} \tag{38}$$

where $\boldsymbol{E}_{\mathrm{CO}}$ and $\boldsymbol{E}_{\mathrm{CROSS}}$ are the co- and cross-polarized radiation patterns, respectively. It is worth mentioning that Eq. (37) reduces to Eq. (14) for $C_{\mathrm{E}}(\theta_{\mathrm{f}}) = C_{\mathrm{H}}(\theta_{\mathrm{f}}) = C(\theta_{\mathrm{f}})$. In addition, Eq. (38) yields the cross-polarized peaks in the 45° planes, which is consistent with measured data and more sophisticated theoretical models (33). Nevertheless, it is not our intention to analyze feed antennas completely, but rather to present simple analytical models that can be useful to antenna engineers as a first approximation to real feed patterns.

As discussed in the subsection titled “Summary of Main Results,” balanced feeds yield improved performance when illuminating reflector systems. A type of balanced feed antennas widely used in practice is the corrugated conical horn, also often referred to as a *scalar horn* (Fig. 16). Corrugated conical horns present a phase center that is reasonably stable with changing frequency (23,33), in addition to a copolarized pattern that is nearly balanced for practical purposes and can be well modeled by Eqs. (14) and (15) or (21).

The main purpose of using corrugations is to obtain the same boundary conditions around the inside of the horn. For corrugation depths of a quarter wavelength, the short circuit at the bottom is transformed to an open circuit at the top of the corrugation, yielding boundary conditions that appear to be more uniform as the number of corrugations per wavelength increase (20). This yields a symmetric radiation pattern down to as low as -25 dB over a reasonably wide operational bandwidth, typically of 1.6 : 1 or more.

The cross-polarized pattern, however, may contain peaks in the 45° planes, similarly to the unbalanced model of Eq. (38). As discussed in the section entitled “Multiple-Reflector Antenna Systems,” and as approximately modeled by Eq. (30), feed XPOL peaks appear in the far-field patterns of dual-reflector systems, even with the enforcement of the conditions given by Eqs. (27) to (29). To minimize feed XPOL, a careful design and construction process must be performed. The corrugation depths must be set properly to achieve resonance, taking into account all dimensions related to the corrugations as well as the general geometry of the horn (23). The process has been successfully accomplished in practice, often also employing sections of tapered and/or dual-depth corrugations, yielding horns presenting balanced copolar patterns and XPOL levels below -35 dB over practical operational bandwidths (23,34).

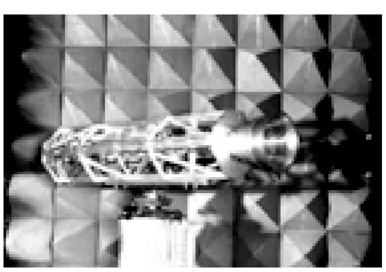

Figure 16. Conical corrugated horn. (Courtesy of Emilio Abud Filho, Brazilian Telecommunications Center for Research and Development.)

Finally, other types of feed antennas are also used in practice, such as wire antennas and pyramidal and sectoral horns (20). The latter are used for illuminating reflectors with elliptical projected apertures, which were discussed previously. In addition, it is common to have an array of horns or other feed antennas illuminating shaped reflectors or large reflectors, such as radio telescopes. This is because the array yields better control of the phase distribution employed to illuminate the reflector, enhancing beam contour and beam scanning performance. A contoured beam is required to illuminate properly a specified region of the earth, as seen from a satellite, and can be accomplished with the shaping of the reflector, one of the topics addressed in the following section.

ADVANCED TOPICS AND RESEARCH

Reflector Antenna Upgrading

During the past few decades reflector antenna designs have evolved through several configurations to increase performance and/or reduce structural complexity. Electrical parameters that are of prime interest are aperture efficiency, SLL, and, more recently, XPOL. All topics herein discussed apply to the various types of reflectors previously addressed. However, the offset configuration is likely to retain, in the near future, the largest percentage of the reflector antenna market.

We first focus our attention on XPOL. Reflector antennas presenting low XPOL (e.g., XPOL ≤ -35 dB) are necessary for frequency-reuse applications, in which an overlap of orthogonally polarized channels is permitted. Many efforts are being conducted to develop these kinds of antennas for mass production (7,35). Dual offset reflectors can be designed for low-cost construction, provided that specific manufacturing constraints are carefully taken into account (7), an effort only possible due to increased interest from industry. Single offset reflector systems illuminated by a matched feed (23) or a feed with a lens (35) can also be designed to satisfy stringent requirements on XPOL, yielding very compact designs. In the latter case, the lens is designed to replace the subreflector, and in both cases bandwidth performance is not as straightforwardly obtained as with the dual reflector configuration. Research continues to be conducted within the area, yielding innovative solutions that provide satisfactory XPOL performance while attending to practical manufacturing specifications. Cost-effective solutions normally require that attendance to a particular specification, such as low XPOL, be achieved with minimal capital outlay, which implies using the maximum amount of infrastructure and technology already implemented. As mentioned previously, there is a tendency to employ existing molds for the main reflector, a concept referred to as *reflector upgrading* (7).

Within this context, existing single offset reflector molds are normally used to construct the main reflector of a dual configuration. However, many such molds are for just fully offset geometries, which, in general, produce a dual reflector configuration that is Gregorian with the feed axis z_f intersecting the main reflector (Fig. 11). The same problem may also occur in certain Gregorian configurations even when the main reflector is not just fully offset. The final design should provide suitable clearance between the bottom of the main reflector and the feed axis in order to access the feed antenna with a straight section of waveguide, thus reducing the complexity and cost of the manufacturing process. This setup is achieved by rotating the parent ellipsoid (i.e., the conical surface from which the subreflector is generated) until the desired clearance is obtained. The rotation is performed in such a way that the feed remains pointed toward the intersection of the new subreflector and the ray coming from the center of the main reflector, thus avoiding the introduction of spillover and phase errors. The amount of rotation β_R that yields a desired angle γ' between the main reflector and feed axes can be determined from (7)

$$\frac{\dfrac{1+e}{1-e\cos(180^\circ-\beta-\beta_R-\psi_C)}f_S}{2(c+f_S)-\dfrac{1+e}{1-e\cos(180^\circ-\beta-\beta_R-\psi_C)}f_S}\sin(180^\circ-\beta-\beta_R-\psi_C)=\sin(\beta+\beta_R+\gamma') \quad (39)$$

Given the initial configuration and the desired angle γ', Eq. (39) can be solved to determine β_R. In general, values for γ' smaller than the one used in the original configuration bring the feed axis away from the main reflector. However, the nonconventional design obtained after the rotation of the parent ellipsoid may lead to a XPOL degradation due to the fact that the minimum-XPOL conditions, Eqs. (27) to (29), are no longer satisfied. A simple solution to this problem is to alter the value of the subreflector eccentricity while keeping all orientation angles constant. In general, eccentricity values greater than the one employed before the rotation will reduce the system XPOL (7), yielding a low-cross-polarization dual offset Gregorian antenna that has adequate clearance between the feed axis and the bottom of the main reflector. In addition, the resulting configuration has the ability to operate with either a linearly polarized or a circularly polarized feed over a wide bandwidth without the need to be repositioned (no substantial beam squint).

Compact designs for reflector systems have been investigated for years. It is desirable, for example, to upgrade a main reflector with a subreflector that is as small as possible. In addition, with the proliferation of satellite TV at Ku band employing single offset reflector systems for reception, there is now interest in minimizing the size of the reflector while maintaining required gain performance. This is only possible by increasing aperture efficiency through the reduction of diffraction effects and feed blockage. High-performance feeds are also necessary, especially if they are located close to the reflector, as in a very compact design requiring a complete near-field analysis. Finally, microelectronics technology is integrating both low- and high-frequency hardware into the feed system. It is common nowadays to find feeds that already include low-noise amplifiers, downconverters, and other electrical devices in a single unit.

Shaped, Deployable, and Frequency-Selective Reflector Surfaces

Reflector antennas can be shaped to improve gain and aperture efficiency (e.g., Fig. 3). The basic concept is to shape the subreflector of a dual-reflector system to obtain the desired amplitude distribution at the main reflector projected aperture, normally nearly uniform for maximizing gain, and then shape the main reflector to recover the uniform phase distribution, which was disturbed by shaping the subreflector. Resulting aperture efficiencies are usually in the range of 70% to 80%, although higher values have been reported for dual shaped offset systems (11). The fundamental tradeoff that antenna designers must face, in this case, is the achievement of such efficiencies while still obtaining satisfactory sidelobe levels.

Another topic certain to continue receiving attention in the coming millenium is the shaping of single-reflector systems for contoured beam applications. A contoured beam is necessary to illuminate specific regions of the earth efficiently from a satellite. This avoids unnecessary coverage of regions outside the satellite main service area. Reflector shapes for contoured beam and high-gain applications, especially for the offset case, are normally obtained numerically through elaborate synthesis and optimization processes (3–5,9,10), which include the feed antenna or array. Equation (17) can be used to set the initial positions for the feed antennas (3). Also important is mathematical and numerical modeling of the surfaces to yield results that can be implemented in practice (36). Feed arrays are also used with reconfigurable mesh surfaces and deployable reflectors to enhance performance (1).

Reconfigurable shapes, deployable reflectors, and polarization- or frequency-selective surfaces require an in-depth study of electrical and magnetic materials, which show that reflector antenna engineering is not possible without large interdisciplinary activities. Frequency-sensitive surfaces, for example, reflect only radiation in specific frequency bandwidths (1). A four-frequency reflector system has been used for the ESA–NASA Cassini mission to Titan, the largest moon of Saturn (1). The subreflector carried by the Voyager spacecrafts shown in Fig. 3 is another example; it is transparent to radiation at S band and reflecting at X band. The subreflector was manufactured with X-band resonant aluminum crosses etched on a Mylar sheet, yielding reflecting and transmitting losses lower than 0.1 dB.

Reflectors that can be deployed in space deserve distinct attention. The classical solution is the so-called umbrella reflector (1), which works well for axisymmetric configurations. An idea that seems promising for the offset case is a configuration that opens like a manual fan. In addition, inflatable reflectors have been investigated over the past few years, with the successful construction and testing of a few prototypes.

Neural Networks, Fuzzy Logic, and Genetic Algorithms Applied to the Synthesis of Reflector Antennas

As we have seen, reflector antenna applications range from very specific and unique systems, such as deployable reflectors and radiotelescopes (see the subsection on the Green

Bank Radio Telescope), to large-scale production for commercial systems, such as earth terminals in VSAT networks and small receiving antennas for satellite TV. In addition, reflector antennas are also used in radar systems and other devices directly related to electronic warfare and defense. Due to the wide range of applications and commercial importance, it is essential to have reliable alternative algorithms to design effective reflector configurations. Analytical and numerical tools that have recently been used with applied electromagnetics and appear to work well for the synthesis of reflector antennas, although they are most familiar in other areas such as controls and signal processing, include neural networks, fuzzy logic, and genetic algorithms (37–40).

The basic idea of using neural networks for designing reflector antennas is as follows: First one relates a few radiation patterns, or other parameters of interest, directly to the reflector geometries that generated them according to a previously selected analysis algorithm. This process is normally referred to as *training* the neural network. Once the training is completed, the desired radiation pattern is employed as the input parameter, so that the neural network yields the corresponding reflector geometry. Finally, the selected analysis technique is used on the resulting geometry to validate the process. This type of synthesis has been successfully implemented to determine reflector shapes for contoured beam applications (37). Reflector antenna synthesis based on neural networks is normally very fast, because analysis techniques are required only for the training of the network.

Also currently under investigation is the effectiveness of using neural networks at a real-time level to reduce XPOL, noise, and interference in single offset reflector systems. Fuzzy logic can be applied to the synthesis and enhancement of reflector antenna systems in a similar manner, although there are certain inherent differences not addressed herein (38).

Genetic algorithms (GAs), on the other hand, rely on an optimization search to elect a suitable design. The initial set of configurations, referred to as the basis *population,* is formed by relating random designs to *chromosomes,* each one formed by a sequence of binary numbers that define the corresponding reflector geometry. A figure of merit is then associated with each chromosome, becoming higher as the electrical performance of the configuration comes closer to the desired one. Chromosomes with the highest figures of merit are selected to cross with the remaining ones, a process called *crossover* (39,40). In addition, the best chromosomes (i.e., the ones with the highest figures of merit) are often duplicated before crossover, eliminating the worst ones, a procedure referred to as *natural selection* (39,40). After the crossover is completed, a few binary numbers in a subset of chromosomes can be randomly altered, simulating the process of *mutation* in biological evolution. All figures of merit are then recomputed, and the whole process is repeated if the desired performance has not been achieved.

The aforementioned procedure is a basic description of a genetic algorithm, although variants are often encountered in practice (39,40). A major advantage of GAs over other optimization techniques is that once the process has converged, more than one configuration attending the desired performance is often encountered. It is also common to find configurations that are very different from classical solutions and could not be easily conceived through straightforward reasoning. Practical manufacturing constraints can then be considered for choosing the most adequate reflector antenna configuration.

ACKNOWLEDGMENTS

The author is deeply indebted to George Behrens (National Radio Astronomy Observatory) and Nick Moldovan (Prodelin Corporation), as well as to their institutions, for providing many illustrations and photographs reprinted in this work. The author likewise thanks NASA/JPL and the Brazilian Telecommunications Center for Research and Development (CPqD/TELEBRAS).

BIBLIOGRAPHY

1. W. V. T. Rusch, The current state of the reflector antenna art—entering the 1990's, *Proc. IEEE,* **80**: 113–126, 1992.
2. S. Silver (ed.), *Microwave Antenna Theory and Design,* New York: McGraw-Hill, 1949.
3. Y. Rahmat-Samii, Reflector antennas, in Y. T. Lo and S. W. Lee (eds.), *Antenna Handbook,* New York: Van Nostrand Reinhold, 1988.
4. C. Scott, *Modern Methods of Reflector Antenna Design,* Norwood, MA: Artech House, 1990.
5. P. S. Kildal, Synthesis of multireflector antennas by kinematic and dynamic ray tracing, *IEEE Trans. Antennas Propag.,* **38**: 1587–1599, 1990.
6. K. W. Brown, Y. H. Lee, and A. Prata, Jr., A systematic design procedure for classical offset dual reflector antennas with optimal electrical performance, in *IEEE Antennas Propag. Soc. Symp. Dig.,* Ann Arbor, MI, 1993, pp. 772–775.
7. M. A. B. Terada and W. L. Stutzman, Computer-aided design of reflector antennas, *Microw. J.,* **38** (8): 64–73, 1995.
8. W. V. T. Rusch and P. D. Potter, *Analysis of Reflector Antennas,* New York: Academic, 1970.
9. A. W. Love (ed.), *Reflector Antennas,* Piscataway, NJ: IEEE Press, 1978.
10. B. S. Westcott, *Shaped Reflector Antenna Design,* London: Wiley, 1983.
11. A G. Cha, Preliminary announcement of an 85 percent efficient reflector antenna, *IEEE Trans. Antennas Propag.,* **31**: 341–342, 1983.
12. A. H. Rana, J. McCoskey, and W. Check, VSAT technology, trends, and applications, *Proc. IEEE,* **78**: 1087–1095, 1990.
13. A. C. Ludwig, The definition of cross polarization, *IEEE Trans. Antennas Propag.,* **21**: 116–119, 1973.
14. TICRA Eng., *GRASP7—Single and Dual Reflector Antenna Program Package,* Copenhagen, Denmark.
15. M. A. B. Terada and W. L. Stutzman, Design of offset-parabolic-reflector antennas for low cross-pol and low sidelobes, *IEEE Antennas Propag. Mag.,* **35** (6): 46–49, 1993.
16. A. W. Rudge and N. A. Adatia, Beam squint in circularly polarized offset parabolic reflector antennas, *Electron. Lett.,* **11**: 513–515, 1975.
17. D. W. Duan and Y. Rahmat-Samii, Beam squint determination in conic-section reflector antennas with circularly polarized feeds, *IEEE Trans. Antennas Propag.,* **39**: 612–619, 1991.
18. W. L. Stutzman, *Polarization of Electromagnetic Systems,* Norwell, MA: Artech House, 1993.

19. M. A. B. Terada and W. L. Stutzman, Cross polarization and beam squint in single and dual offset reflector antennas, *Electromagnetics J.,* **16**: 633–650, 1996.
20. W. L. Stutzman and G. A. Thiele, *Antenna Theory and Design,* 2nd ed., New York: Wiley, 1998.
21. A. G. P. Boswell and R .W. Ashton, Beam squint in a linearly polarized offset parabolic reflector, *Electron. Lett.,* **12**: 596–597, 1976.
22. P. S. Kildal, Diffraction analysis of a proposed dual-reflector feed for the spherical reflector of the Arecibo observatory, *Radio Sci.,* **24**: 601–617, 1989.
23. A. W. Rudge et al. (eds.), *The Handbook of Antenna Design,* Stevenage, UK: Peregrinus, 1982.
24. W. V. T. Rusch et al., Derivation and application of the equivalent paraboloid for classical offset Cassegrain and Gregorian antennas, *IEEE Trans. Antennas Propag.,* **38**: 1141–1149, 1990.
25. B. Shen and W. L. Stutzman, A scanning tri-reflector antenna with a moving flat mirror, *IEEE Trans. Antennas Propag.,* **43**: 270–276, 1995.
26. C. Dragone, Offset multireflector antennas with perfect pattern symmetry and polarization discrimination, *Bell Syst. Tech. J.,* **57**: 2663–2684, 1978.
27. Y. Mizugutch, M. Akagawa, and H. Yokoi, Offset dual reflector antenna, *IEEE Antennas Propag. Soc. Symp. Dig.,* Amherst, MA, 1976, pp. 2–5.
28. S. Srikanth, Comparison of spillover loss of offset Gregorian and Cassegrain antennas, *IEEE Antennas Propag. Soc. Symp. Dig.,* London, Canada, 1991, pp. 444–447.
29. M. A. B. Terada and W. L. Stutzman, Computer-aided design of reflector antennas: The Green Bank radio telescope, *IEEE Trans. Microw. Theory Tech.,* **46**: 250–253, 1998.
30. P. H. Pathak, Techniques for high-frequency problems, in Y. T. Lo and S. W. Lee (eds.), *Antenna Handbook,* New York: Van Nostrand Reinhold, 1988.
31. Y. Rahmat-Samii and V. Galindo-Israel, Shaped reflector antenna analysis using the Jacobi–Bessel series, *IEEE Trans. Antennas Propag.,* **28**: 425–435, 1980.
32. W. L. Stutzman, S. W. Gilmore, and S. H. Stewart, Numerical evaluation of radiation integrals for reflector antenna analysis including a new measure of accuracy, *IEEE Trans. Antennas Propag.,* **36**: 1018–1023, 1988.
33. P. J. B. Clarricoats and A. D. Olver, *Corrugated Horns for Microwave Antennas,* Stevenage, UK: Peregrinus, 1984.
34. S. Ghosh, E. Kuhn, and A. Prata, Simplified high-performance dual-banded feed comprising a dual-depth corrugated launcher and a conventional horn, *Electron. Lett.,* **20**: 532–533, 1984.
35. E. Lier and S A. Skyttemyr, A shaped single reflector offset antenna with low cross polarization fed by a lens horn, *IEEE Trans. Antennas Propag.,* **42**: 478–483, 1994.
36. J. R. Bergmann et al., Synthesis of shaped-beam reflector antennas patterns, *IEE Proc.,* part H, **135**: 48–53, 1988.
37. G. Washington, Aperture antenna shape prediction by feedforward neural networks, *IEEE Trans. Antennas Propag.,* **45**: 683–688, 1997.
38. J. S. R. Jang and C. T. Sun, Neuro-fuzzy modeling and control, *Proc. IEEE,* **83**: 378–406, 1995.
39. D. S. Weile and E. Michielssen, Genetic algorithm optimization applied to electromagnetics: A review, *IEEE Trans. Antennas Propag.,* **45**: 343–353, 1997.
40. J. M. Johnson and Y. Rahmat-Samii, Genetic algorithms in engineering electromagnetics, *IEEE Antennas Propag. Mag.,* **39** (4): 7–25, 1997.

MARCO A. B. TERADA
University of Brasilia

REFLECTOR RADAR ANTENNAS. See RADAR ANTENNAS.